
This is an electronic reprint of the original article.
This reprint may differ from the original in pagination and typographic detail.

Yuan, Xiaolei; Heikari, Lassi; Hirvonen, Janne; Liang, Yumin; Virtanen, Markku; Kosonen, Risto; Pan, Yiqun

System modelling and optimization of a low temperature local hybrid energy system based on solar energy for a residential district

Published in:
Energy Conversion & Management

DOI:
[10.1016/j.enconman.2022.115918](https://doi.org/10.1016/j.enconman.2022.115918)

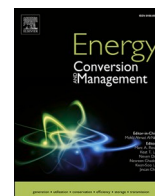
Published: 01/09/2022

Document Version
Publisher's PDF, also known as Version of record

Published under the following license:
CC BY

Please cite the original version:
Yuan, X., Heikari, L., Hirvonen, J., Liang, Y., Virtanen, M., Kosonen, R., & Pan, Y. (2022). System modelling and optimization of a low temperature local hybrid energy system based on solar energy for a residential district. *Energy Conversion & Management*, 267, Article 115918. <https://doi.org/10.1016/j.enconman.2022.115918>

This material is protected by copyright and other intellectual property rights, and duplication or sale of all or part of any of the repository collections is not permitted, except that material may be duplicated by you for your research use or educational purposes in electronic or print form. You must obtain permission for any other use. Electronic or print copies may not be offered, whether for sale or otherwise to anyone who is not an authorised user.



System modelling and optimization of a low temperature local hybrid energy system based on solar energy for a residential district

Xiaolei Yuan^{a,b,*}, Lassi Heikari^a, Janne Hirvonen^a, Yumin Liang^b, Markku Virtanen^a, Risto Kosonen^{a,c}, Yiqun Pan^b

^a School of Engineering, Aalto University, P.O. Box 14400, FI-00076 Espoo, Finland

^b School of Mechanical Engineering, Tongji University, 4800 Cao'an Road, 201804 Shanghai, China

^c College of Urban Construction, Nanjing Tech University, 211816 Nanjing, China

ARTICLE INFO

Keywords:

Solar energy
Seasonal thermal energy storage
Local hybrid energy system
Multi-objective optimization
Energy cost saving
Carbon reduction

ABSTRACT

Utilizing solar energy for heat supply can reduce CO₂ emissions and mitigate global climate change. In the Nordic region (e.g., Iceland and Finland), a tremendous seasonal mismatch exists between the availability of solar radiation and building heating demand. This paper proposes a local hybrid energy system based on solar energy for a residential district. It applies a borehole thermal energy storage to store solar energy in non-heating seasons, and uses stored energy for part of total heating demand in a residential neighbourhood in heating seasons. Photovoltaic panels are used to generate electricity for heat pump operation. To find out cost-optimal and eco-friendly solutions, the local energy system was first modelled and simulated in TRNSYS. Then, genetic algorithms were applied to optimize the system performance and costs. In optimal solutions, 38%–58% of total heating demand could be covered by on-site heat energy with the levelized cost of energy of 110–184 €/MWh. On this basis, importing additional electricity from grid to increase the utilization rate of air-to-water heat pumps can further increase the on-site heat energy fraction to 41%–88% with the levelized cost of energy of 108–201 €/MWh. Compared with the situation of fully district heating input, the proposed system can annually reduce CO₂ emissions by 102–217 tons with the rate of 31–66%. Although the initial cost of the studied system is higher than that of district heating, the local hybrid energy system is worth further developing considering decentralizing heat energy production and reducing CO₂ emissions.

1. Introduction

Fossil energy sources (e.g., coal, oil and natural gas) have largely promoted the development of global economy and human living standards, but are followed by huge carbon emissions adversely deteriorating the environment (e.g., climate change and ecological imbalance) [1] and human welfare [2]. Compared with the average concentration of global atmospheric CO₂ of 280 ppm before the industrialization, in 2020 it increased to 412.5 ppm [3]. CO₂ emissions from building sector reached 10 Gt in 2019, which was 28% of global energy-related emissions [4]. Building sector has exceeded the transportation and industrial sectors, and become the biggest energy consumer globally. Thus, to achieve carbon neutrality by 2050, all newly-built buildings and 20% of existing buildings are required to achieve zero carbon emissions as soon as possible before 2030 [5]. Building sector in European Union (EU) accounts for a 40% share of the total energy consumption, around 55%

of which is used for building space heating (SH), space cooling (SC) and domestic hot water (DHW) heating [6]. Due to the depletion of primary energy and corresponding environmental problems, renewable energy sources are widely developed and utilized to replace fossil fuels for carbon emission reduction and global warming restriction [7].

Solar energy is one of the commonly used renewable energy sources, which has been widely utilized for heating (i.e., solar thermal collectors [8]) and electricity generation (i.e., photovoltaic panels [9]) during past decades. Solar photovoltaic (PV) system has the advantages of modularity, easy maintenance and relatively long lifetime [10]. However, the amount of solar energy is related to the geographical location [11] and the solar radiation conditions are also different between summer and winter [12]. In high latitude areas (e.g., Finland), utilizing solar energy for heating is a challenge, as there is a seasonal mismatch between the solar radiation and heating demand [13]. The summer with the highest solar radiation has the lowest building heating demand, while the winter with the lowest solar radiation has the highest heat demand. To balance

* Corresponding author.

E-mail address: xiaolei.yuan@aalto.fi (X. Yuan).

<https://doi.org/10.1016/j.enconman.2022.115918>

Received 7 March 2022; Received in revised form 1 June 2022; Accepted 19 June 2022

Available online 24 June 2022

0196-8904/© 2022 The Author(s). Published by Elsevier Ltd. This is an open access article under the CC BY license (<http://creativecommons.org/licenses/by/4.0/>).

Nomenclature		T_{LC}	Life cycle time, year
Symbols		x_i	Decision variables
A_{PV}	The area that PV panels can be installed, m^2	Abbreviations	
$C_{e,export}$	Hourly surplus electricity selling profit, €	AHU	Air handling unit
$C_{e,import}$	Hourly costs for imported electricity, €	AW-HPs	Air-to-Water Heat Pumps
$C_{I,t}$	Investment costs in year t , €	BTES	Borehole Thermal Energy Storage
$C_{M,t}$	Maintenance costs in year t , €	COP	Coefficient of Performance
$C_{O,t}$	Operation costs in year t , €	DH	District Heating
E_{demand}	Building total heating energy demand, MWh	DHW	Domestic Hot Water
$E_{DH,import}$	Heat energy imported from DH, MWh	GA	Genetic Algorithm
$E_{e,export}$	Hourly exported electricity, MWh	HP	Heat Pump
$E_{e,import}$	Hourly imported electricity, MWh	LCC	Life Cycle Cost
$E_{grid,import}$	Electricity imported from the grid, MWh	LCOE	Levelized Cost of Energy
E_t	Amount of heat energy produced, MWh	LEHR	Load Effective Hour Rate (%)
$l_{i,max}$	upper limit for decision variable x_i	MOO	Multi-Objective Optimization
$l_{i,min}$	lower limit for decision variable x_i	OHEF	On-site Heat Energy Fraction
$P_{CF,buying}$	Electricity buying commission fee, €/MWh	PTES	Pit Thermal Energy Storage
$P_{CF,selling}$	Electricity selling commission fee, €/MWh	PV	Photovoltaic
$P_{e,buying}$	Hourly electricity buying price, €/MWh	REF	Renewable Energy Fraction
$P_{e,distribution}$	Electricity distribution price, €/MWh	SC	Space Cooling
P_{Elspot}	Hourly Nordpool Elspot price, €/MWh	SH	Space Heating
$P_{e,selling}$	Hourly electricity selling price, €/MWh	STES	Seasonal Thermal Energy Storage
$P_{e,tax}$	Electricity tax, €/MWh	TTES	Tank Thermal Energy Storage
$A_{PV}(x)$	The area that PV panels can be installed, m^2	VAT	Value added tax
r	The interest rate, %	VH	Ventilation Heating
		WW-HPs	Water-to-Water Heat Pumps

the solar energy conversion heating and building heating demand, solar energy has to be stored somehow in summer, and used for heating demand in winter.

Seasonal thermal energy storages (STESs) are possibly used to balance the mismatch between renewable energy supply and thermal demand [14]. Salvestroni et al. designed a solar district heating system for a community in Italy and the solar fraction reached up to 44% with an optimized configuration of STESs [15]. In review, Mahon et al. [16] classified STESs into open loop systems (e.g., pit thermal energy storage (PTES) and tank thermal energy storage (TTES)) and closed-loop systems (e.g., borehole thermal energy storage (BTES)). PTES excavates a large pit into the ground, and fills it with water as the storage media so that the ground is easy to excavate [17]. TTES stores thermal energy with tanks made of reinforced concrete, steel or glass fibre reinforced plastic, and also uses water as the media [18]. Unlike PTES, TTES can be either fully or partly excavated into the ground, or even can be located above the ground. BTES stores thermal energy using a closed-loop heat exchange system in soil or rock below the ground [16]. Lim et al. [19] introduced a typical BTES system, which consists of borehole heat exchangers installed with single or double U-pipes, a heat source, and a buffer tank for charging and discharging. Different from PTES and TTES, water-glycol mixture is usually used as heat transfer fluid in BTES to avoid freezing. BTES is considered a flexible solution for STES due to its wide implementation on various grounds. The ground itself, actually working as the storage media, has a relatively stable temperature, and creates favourable conditions for both heat storage and discharge to use directly or through heat pumps (HPs) [20].

Del Amo et al. [21] integrated the HP heating system with solar PV/thermal collectors and a seasonal storage system. Taking an educational building in Spain as a case study, the system achieves a solar fraction of 60%. Beausoleil-Morrison et al. [22] simulated a single building-scale solar thermal system with seasonal storage in a cold climate area for SH and DHW heating. Solar fraction of 87–98% is achieved with the solar collector area of $41.6 m^2$, and the seasonal storage volume of $36 m^3$. However, STES technologies are generally less feasible in an

individual building as the small storage size is not functional. Thus, the hybrid energy system integrating solar energy utilization with STES is more potential to be implemented at neighborhood level for higher profitability and operating efficiency.

Kubiński et al. [23] gave attention to the district heating (DH) system and dynamically modelled the cooperation among solar thermal collectors with seasonal storage, conventional industrial boilers and traditional DH network. Schach et al. [24] compared a decentralized heat supply system with seasonal storage connected to solar thermal collectors and a gas-heated system, and found the cost of a decentralized heat supply system is not much different from that of the traditional gas-heated system after economic analysis. Saloux et al. [25] proposed a model-based predictive control strategy for the hybrid energy system at a solar community, where solar energy is collected by solar thermal collectors and stored seasonally with BTES, and they found the control strategy saves 38% of system cost and 32% of greenhouse gas emissions.

The above systems all utilize solar energy to produce heat energy directly with solar thermal collectors; but the solar communities producing heat energy with PV thermal HPs have more potential than communities equipped with solar thermal collectors. The air source HPs can maintain stable operation and high efficiency when the ambient temperature is relatively high during the day, exactly when the solar power is at its peak. Thus, using air source HPs as the medium for absorbing low-grade heat in the air to heat cold water, the PV thermal HPs system can utilize solar energy to generate heat and electricity at the same time more efficiently than solar thermal collectors [26]. Moreover, the PV power can be either consumed on site for driving HPs or sold to the grid for economic benefits, providing a new idea for district heating. In practice, the economic and efficiency performance of PV thermal HPs combined with STESs becomes the crucial basis for popularizing the system. With the aim to fill the research gap, this paper applied PV panels in the studied hybrid energy system to generate electricity for heat energy production and seasonal storage in a residential neighbourhood for further analysis and optimization.

Since energy conservation and carbon reduction are the main

objectives currently, Gabrielli et al. [27] proposed an optimization algorithm for minimizing the CO₂ emissions and satisfying the thermal demands of given buildings at the same time. Compared with a traditional centralized system, the proposed algorithm can reduce the CO₂ emissions on a campus by up to 87%, with an improvement on 72% reduction achieved with the current operation strategy. Raluy et al. [28] applied the life cycle assessment method in estimating the environmental burden through the whole life cycle of the central solar heating plants with the seasonal storage system. Maximov et al. [29] performed a multi-objective optimization of a solar heating system with seasonal thermal storage based on costs and greenhouse gas emissions as the objectives. Results show that STES improves the system performance by decreasing the emissions by 90% and only increasing the levelized cost of energy (LCOE) by less than 20% compared with a gas-heated system.

This paper studies the hybrid energy system integrating solar energy utilization with STES in a residential neighbourhood, while a low temperature local hybrid energy system is proposed, which uses the stored solar energy in non-heating seasons to cover a part of the total heating demand in the heating season. Then, the proposed system is optimized by genetic algorithms in terms of system performance, economy and carbon emissions. Finally, the feasible and optimal low-temperature local heating solutions, based on solar energy for a residential neighbourhood, are found to meet different optimization goals. Moreover, alternative control options for HPs are analyzed to improve the utilization of on-site heat energy.

Based on the simulation and optimization results of the proposed system, this paper discusses the feasibility of utilizing solar photovoltaic energy to produce and seasonally store heat energy in areas with a tremendous seasonal mismatch between the solar radiation and heating demand. The following research questions are answered: How much on-site produced heat energy fraction and CO₂ emissions reduction can be achieved with the hybrid energy system? Is it beneficial to import grid electricity to produce additional heat energy in a seasonal storage system? What limits the improvement of system performance in a residential neighbourhood? What are the main economic components of the system and the relationship between increased investment and system performance?

2. Methods

2.1. Structure of the study

As shown in Fig. 1, the structure of this study includes two parts, the

dynamic simulation and multi-objective optimization. First of all, the studied local hybrid energy system is described in detail. A residential neighbourhood is introduced, and its hourly thermal demand profiles are obtained using IDA Indoor Climate and Energy (ICE). IDA ICE is a dynamic multi-zone simulation program, which is suitable for modelling (e.g., internal heat gains, HVAC systems and outdoor climate) [30] and can dynamically simulate the mass flows and heat transfer at the same time [31]. Based on the building thermal demand, the whole energy system can be simulated in TRNSYS with all components modelled. After defining indexes to evaluate the system performance, MATLAB is used to read the simulation results and complete the life cycle calculation. Then, multi-objective optimization is performed using the software Multi-Objective Building Optimizer (MOBO) with genetic algorithm. First, optimal solutions for the system are analysed. Next, several alternative control scenarios are simulated and discussed from perspectives of energy production, system costs and CO₂ emission reduction.

2.2. Local hybrid energy system

Fig. 2 shows the schematic map of the system, in which the flow directions are marked with different colours. This section describes in detail the system composition, control strategy and simulation.

2.2.1. System description

The studied local hybrid energy system includes solar energy utilization system, HPs, seasonal storage and so on. The main components of the system are PV panels, air-to-water HPs (AW-HPs), water-to-water HPs (WW-HPs), buffer tank for short time heat energy storage and BTES for seasonal heat energy storage. The operating process of the system is as follows. Firstly, AW-HPs are driven by PV electricity, and provide heat energy to the buffer tank. Then, once the temperature in the tank reaches the upper limit, the heat energy is discharged from the buffer tank to the BTES. Next, the discharge mode mainly operates in wintertime, during which the heat energy is discharged from the BTES to the buffer tank and further to the buildings. Finally, WW-HPs, connecting the BTES and buffer tank, operate during the discharge period to heat the water in the buffer tank so that the required temperature of the building heating network can be met.

The local hybrid energy system was simulated using the commercial dynamic modelling software TRNSYS, while the simulation time was determined based on an overall consideration. The life cycle was assumed as 25 years for the system, but it was infeasible to simulate the whole life cycle for large cases due to the complex system model and

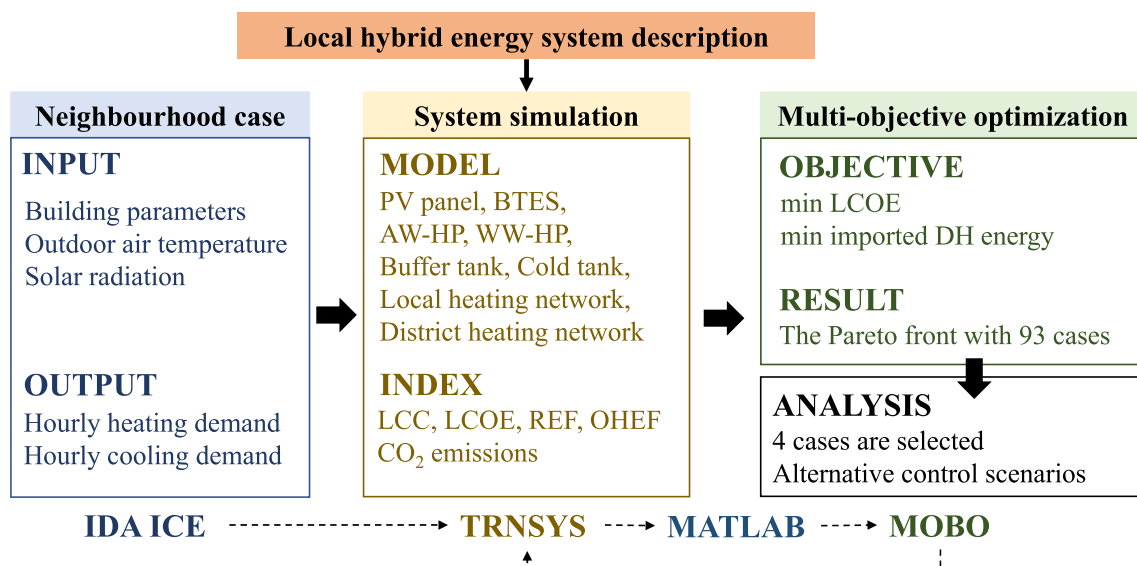


Fig. 1. Structure of the study on the local hybrid energy system.

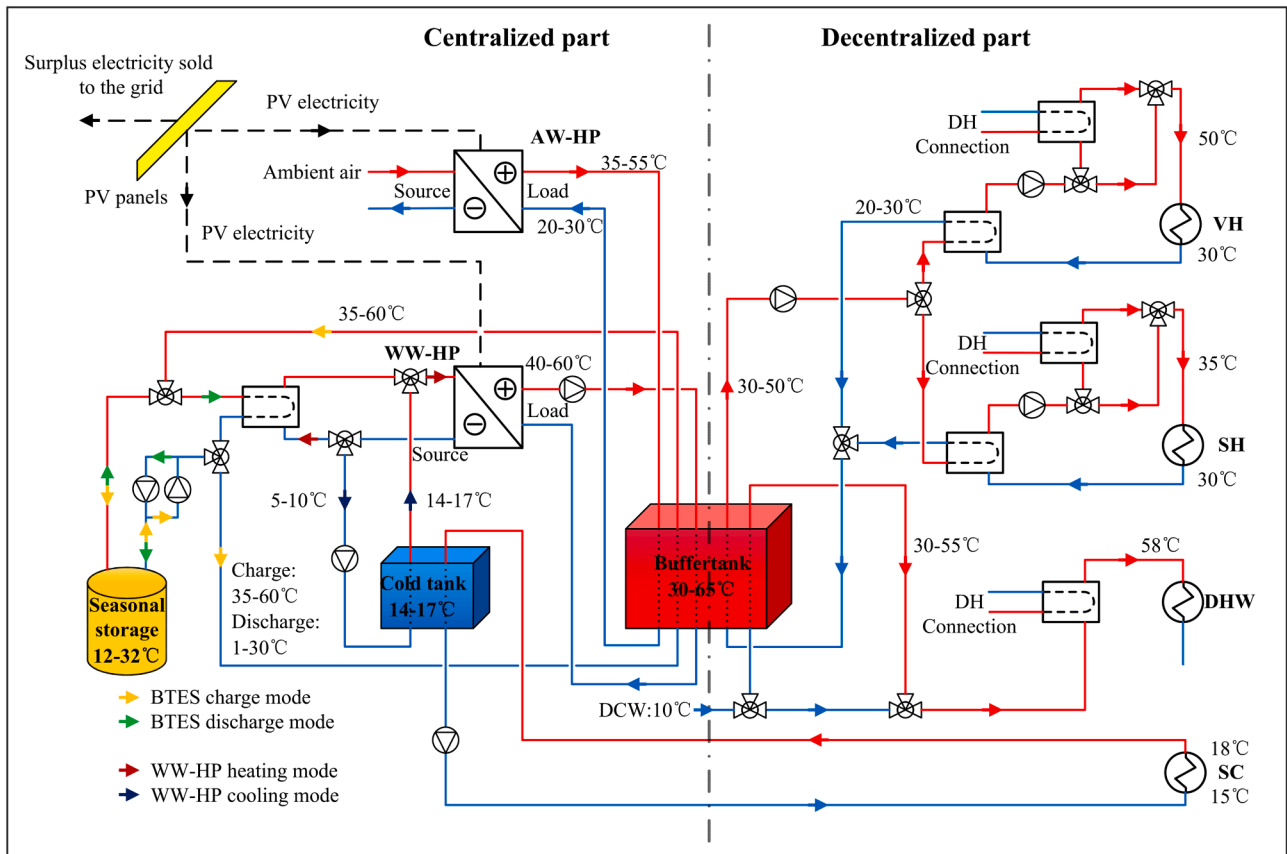


Fig. 2. Schematic map of the studied local hybrid energy system.

relatively long simulation time. In addition, the BTES required a heat-up time for few years to reach the final temperature level, which made the one-year simulation unacceptable. After preliminary simulations for various cases, it was observed that the curves of BTES temperature fluctuations showed no significant differences between in and after the fourth year. Thus, the simulation time was determined as 4 years with the time step set as 7.5 mins, and the operation conditions for the rest of the years were assumed to be similar to that of the fourth year.

2.2.2. System control logic

The system control logic is mainly dependent on the temperature of the buffer tank. Fig. 3 shows the effect of temperature variation on the operation of different components. Firstly, electricity generated by the PV panel will drive the AW-HPs if there is a heat demand in the buffer tank. The heat demand in the tank is based on the tank temperature, so the temperature below 50 °C in the tank will bring this heat demand. However, when the tank temperature exceeds 55 °C, heat is needed no longer and AW-HPs are out of service. The buffer tank starts to discharge

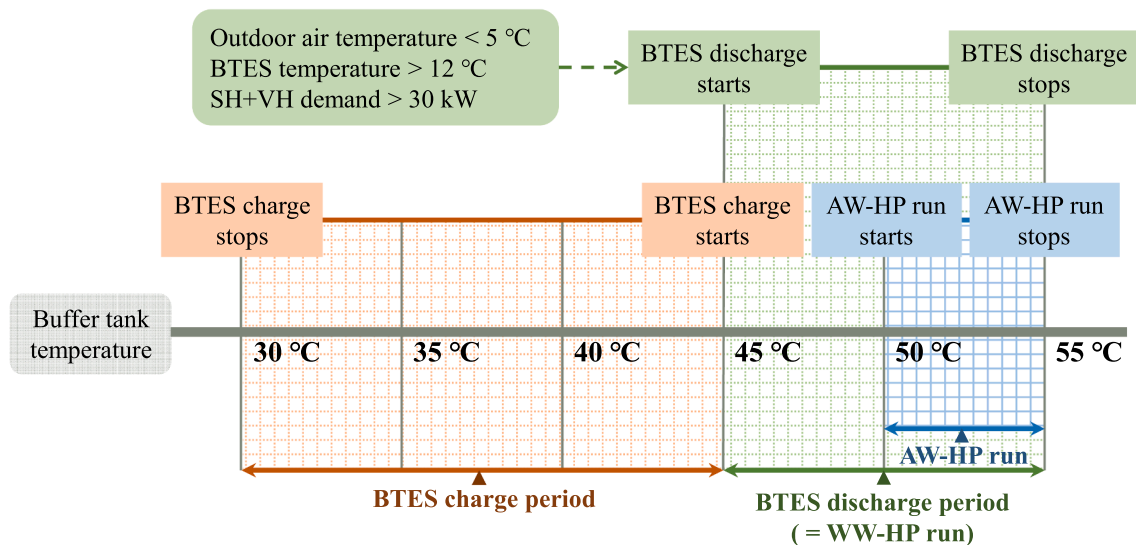


Fig. 3. Control logic for components depending on the buffer tank temperature.

the heat energy to the BTES for seasonal storage when the temperature is above 45 °C and stops when the tank temperature drops to 30 °C.

As the system is only designed to cover some share of annual total heating demand, it is more reasonable to utilize the on-site heat energy during the high heating demand period. Thus, the BTES only discharges heat energy when the sum of SH and VH demand exceeds 30 kW and the outdoor air temperature is below 5 °C. When the heat demands are below 30 kW (mainly happens in late spring or early autumn), they are covered by district heat with relatively lower DH prices, meanwhile, there is a higher potential to run AW-HPs to charge BTES at that time. BTES discharge mode is also controlled based on the buffer tank temperature. The BTES begins to discharge heat when the tank temperature drops under 45 °C, and stops discharging when the tank temperature rises to 55 °C. In addition, if the BTES temperature drops below 12 °C, the discharge will also cease, to avoid excessive cooling. The discharging is restricted until the BTES temperature rises to 14 °C. Time limit exists between the charging and discharging modes, and thus a two-hour break should be set aside from charging mode to discharging one or vice versa.

2.2.3. Thermal demand simulation

Hourly thermal demand profile is important data affecting the design and operation of the hybrid energy system. This paper selected a residential neighbourhood in Espoo, Finland as the studied case, which has 14 eight-storey residential buildings (as shown in Fig. 4) with an altogether floor area of 31100 m². The buildings were newly designed and built according to current regulations of the National Building Code of Finland [32]. Parameters for modelling the residential buildings are summarized in Table 1.

In the residential neighbourhood, the SH network distributes the

Table 1 Building parameters.

Parameter	Unit	Value
U-value of floor	W/(m ² ·K)	0.16
U-value of Ceiling	W/(m ² ·K)	0.09
U-value of External walls	W/(m ² ·K)	0.17
U-value of Doors	W/(m ² ·K)	1.00
U-value of Windows	W/(m ² ·K)	1.00
Indoor temperature	°C	21
Air exchange rate	1/h	0.5
DHW use	l/person/day	56

heat energy to the buildings through underfloor heating, with relatively low operating temperatures. Inlet and outlet temperatures of the SH network depend on the outdoor air temperature, and control curves are needed to control the inlet temperature. The lower the outdoor air temperature is, the higher the heating demand is and the higher the inlet temperature should be. For the under-floor heating system, the control curve is linear as shown in Fig. 5. The critical outdoor air temperature is -26 °C in Espoo [33], below which the SH system must operate with the maximum inlet temperature of 35 °C and the maximum outlet temperature of 30 °C.

Besides the under-floor heating system, there is also a centralized ventilation system in each building, with heating coils in air handling units (AHUs) to heat the air to required temperature before being supplied to the rooms. Generally, the operation temperatures of heating coils in AHU are higher than those of under-floor heating systems, so a separate ventilation heating (VH) network is needed. Design temperatures of the VH network vary for different heating coils. The VH network in this paper operates with the maximum inlet temperature of 50 °C and

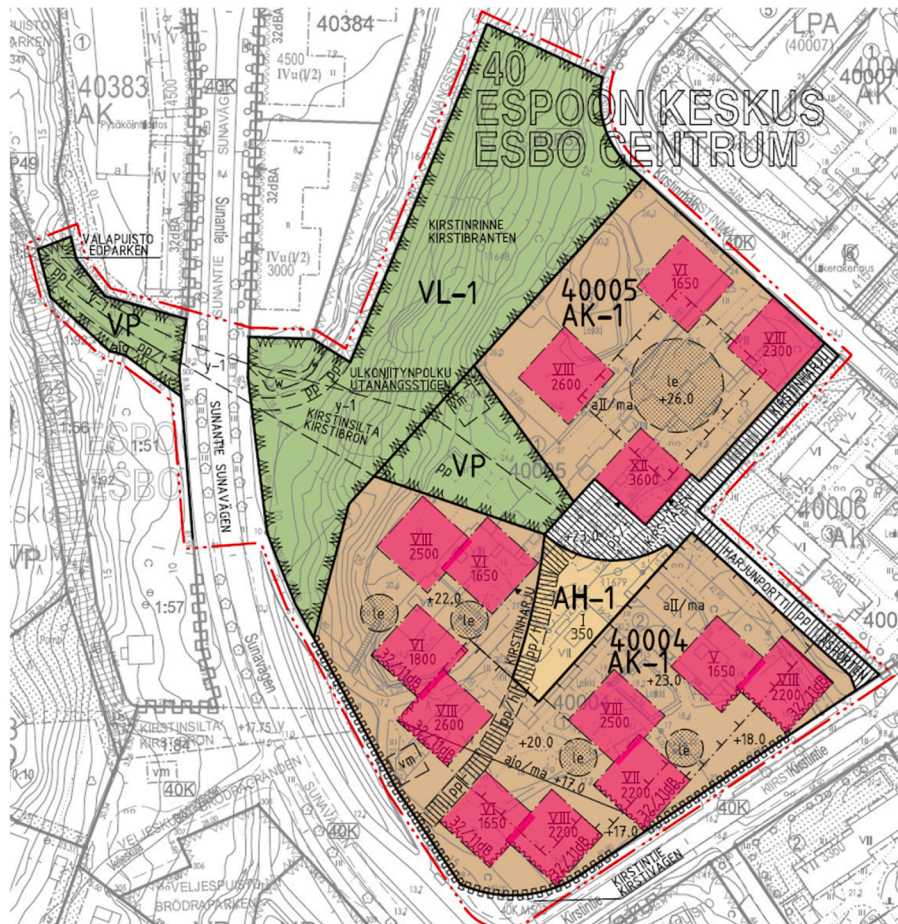


Fig. 4. Studied case of the residential neighbourhood.

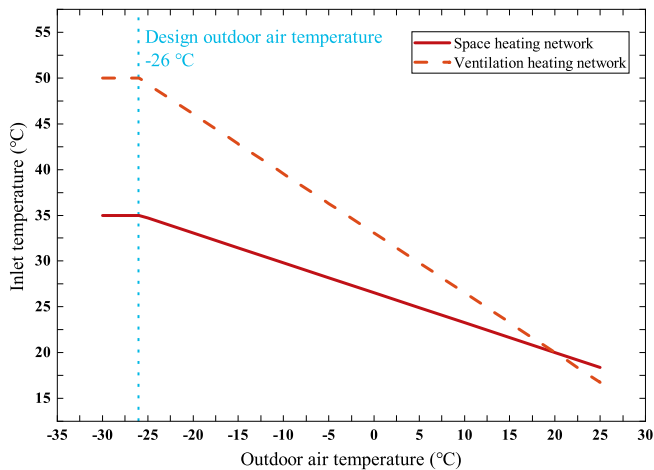


Fig. 5. Inlet temperature control curves for the building heating networks.

the maximum outlet temperature of 30 °C. Inlet and outlet temperatures of the VH network also depend on the outdoor air temperature. Similar to the SH network, a linear control curve is adopted for VH network as shown in Fig. 5.

Weather data (e.g., hourly air temperature, relative humidity, and solar radiation data) are essential inputs to simulate the building heating demand and PV electricity generation. To avoid the possible extreme conditions of the latest data or only one year’s weather data, Test Reference Year 2012 (TRY2012) was adopted in this paper for simulation. Due to the large dimension span and significant differences in weather conditions, Finland is divided into three zones for different weather data, which are I-II (Vantaa), III (Jyväskylä) and IV (Sodankylä). As the area of this studied case is located in Espoo,

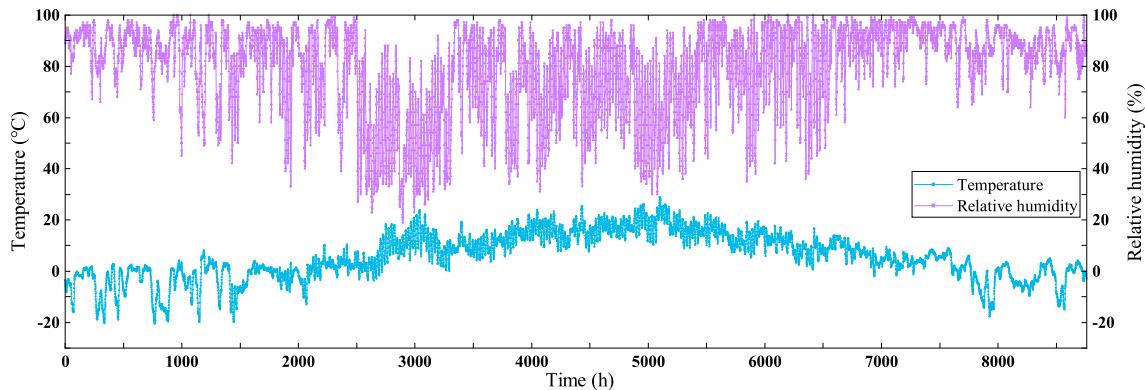
Southern Finland, the I-II weather data was used and the detailed values are shown in Fig. 6. The annual average temperature is 5.63 °C, and the annual total solar radiation on the horizontal surface is 975.02 kWh/m².

After the building parameters and weather data were defined, the building’s hourly thermal demand profile was simulated using IDA ICE software. Although the energy demand between each building varies in reality, it was assumed that energy demand profiles of different buildings were the same in this study. The monthly heating and cooling demand profile of the residential neighbourhood is shown in Fig. 7. On an annual level, DHW heating accounts for the largest share of total heating demand, and remains about half of the total demand during the peak demand months when the SH and VH demand are at a high level. The total annual heating demand of the neighbourhood is 2005 MWh, consisting of 535 MWh of SH demand, 191 MWh of VH demand and 1279 MWh of DHW demand. The total annual cooling demand of the district is 179 MWh for SC, which is relatively lower than the heating demand.

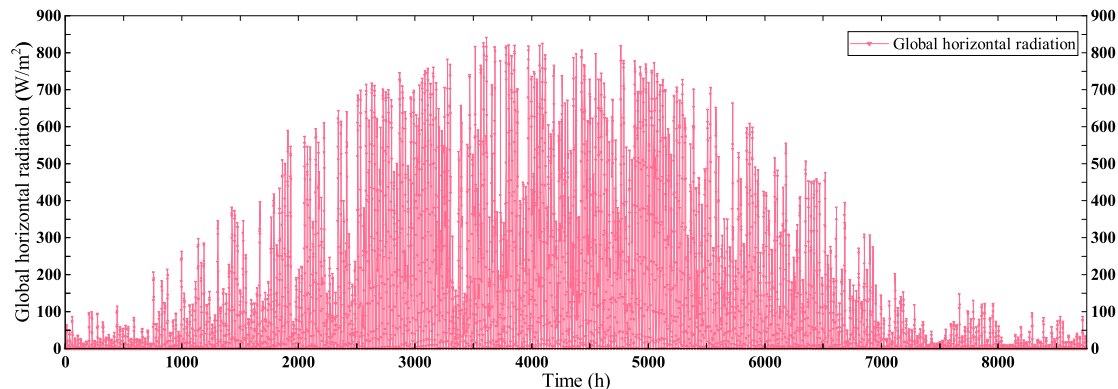
As mentioned in Section 1, STES can be applied to balance the seasonal mismatch between solar radiation and building heating demand in winter, while the common STES are PTES, TTES and BTES. The ground in Espoo is mainly hard rock covered with less than 5 m layer of soil [34], which makes it infeasible to implement PTES or TTES due to the high cost of excavation. Moreover, it is also infeasible to locate TTES above the ground considering its large volume and high land costs. Thus, BTES is applied in this residential neighbourhood, whose boreholes can be drilled into hard rocks.

2.2.4. System component modelling

The studied local hybrid energy system is composed of PV panels, HPs including AW-HPs and WW-HPs, BTES for seasonal heat energy storage, buffer tank for short time heat energy storage and other supporting facilities. TRNSYS simulation software was used to simulate the system, while each component was defined and modelled in detail as shown in Table 2.



(a) Temperature and relative humidity.



(b) Global horizontal radiation.

Fig. 6. Weather data in Test Reference Year 2012 (TRY2012).

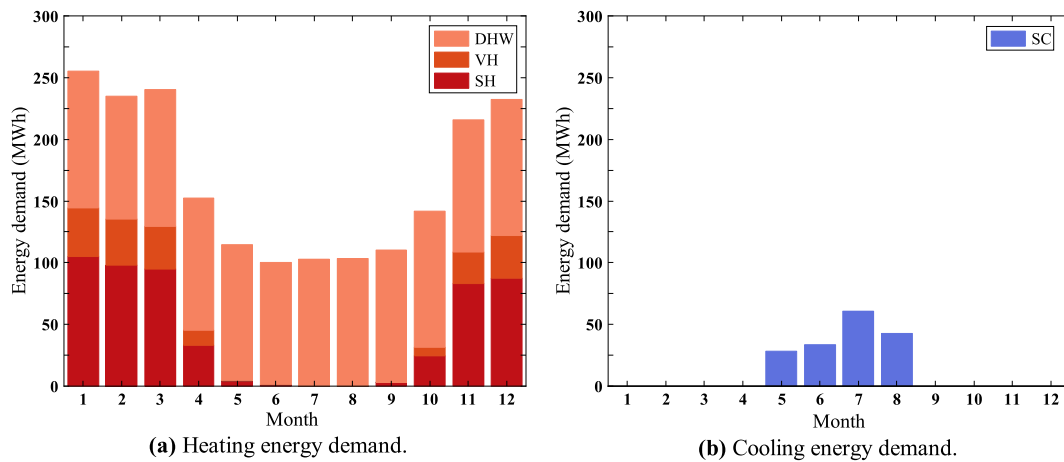


Fig. 7. Monthly thermal demand profile of the residential neighbourhood.

Table 2
Modelling for components of the studied local hybrid energy system.

Component	Model
PV panel	Axitec AC-270P/60S
AW-HP	NIBE F2120-20
WW-HP	NIBE F1345-60
BTES	Type557, the vertical U-tube ground heat exchanger
Buffer tank	Type534, the cylindrical storage tank
Local heating distribution network	Type951, the buried pipe
DH network	Type659, the auxiliary heater
Cold tank	Type534, the cylindrical storage tank

The model of PV panel is Axitec AC-270P/60S with an area of 1.627 m² and the nominal output power of 270 W. PV panels are installed on the flat roof of each building with rooftop area of 290 m². There are altogether 14 buildings in the residential district and the total rooftop area is roughly 4100 m². Considering that there might be also other structural and technical components on the flat roof, only half of the rooftop area was assumed to be occupied by PV panels. Thus, a maximum of 1260 PV panels (90 per building), with a total nominal output power of 340 kW, were utilized and modelled. Inverter efficiency of 90%, reflecting the conversion losses from direct current electricity to alternating current electricity, was taken into consideration [35]. In addition, an annual degradation rate of 0.7% was calculated for the yearly decrease of PV panel power productivity based on an analytical review [36]. As it is hard to define the electricity consumption profiles of the common facility in residential buildings (e.g., elevators, clubrooms, lighting in staircases), the PV power, utilized for the electric loads of the apartments, as well as the electricity storage, are not considered in the system. Instead, the surplus PV electricity is sold to the grid.

AW-HPs and WW-HPs were used in the proposed system. AW-HP was modelled based on properties of NIBE F2120-20 with nominal heat output of 20 kW, while WW-HP was modelled based on properties of NIBE F1345-60 with nominal heat output of 60 kW per HP. Both AW-HPs and WW-HPs can operate in part-load conditions with a minimum part-load ratio of 10%. BTES was modelled with Type 557 (Vertical U-tube ground heat exchanger) in TRNSYS. Technical and thermal parameters of the BTES model are summarized in Table 3. As the average ground temperature in Southern Finland varies between 6 and 8 °C [37], the lowest value was chosen as the initial surface temperature of the storage to ensure the reliability of the modelling.

Local heating distribution network was modelled with the buried pipe Type951 in TRNSYS. For simplicity, the distribution network from the energy station to the buildings was assumed as the star-topology

Table 3
Technical and thermal parameters of the BTES model.

Parameter	Unit	Value	Description	Reference
Header depth	m	5	Thickness of the soil layer above the bedrock	[34]
Radius of borehole	m	0.08	The typical larger borehole radius	[16]
Storage heat capacity	kJ/(m ³ K)	2200	Soil outside the storage is water-saturated gravel.	[39]
Storage thermal conductivity	W/(mK)	3.24	Average value of rock types in Finland.	[40]
Fill thermal conductivity	W/(mK)	0.6	Boreholes filled with water.	[38]
Pipe thermal conductivity	W/(mK)	0.375	U-tube pipes made of polyethylene.	[38]
Flowrate of each loop	kg/h	1200	Recommended value for a similar energy system.	[41]
Fluid density	kg/m ³	936	A mixture of ethylene glycol and water with the proportion of 30%.	[42]
Fluid specific heat	J/(kgK)	3660		
Insulation thermal conductivity	W/(mK)	0.03	Polystyrene boards cover on the top of the storage.	[38]

structure, and there were separate pipes for DHW. The pipes are installed into the gravel with an average ground temperature of around 6.0 °C, and are insulated with plastic foam having the thermal conductivity of 0.03 W/(m·K) [38].

The modelled buffer tank is the cylindrical storage tank Type534 in TRNSYS, while it has a constant height-to-width ratio of 1.5 and is wrapped with a 10 cm layer of mineral wool. The tank was assumed to be excavated into the ground due to its relatively high volume (ranging from 5 × 10⁴ to 2 × 10⁵ m³), and the heat losses from the tank to the outside ground were calculated based on the average ground temperature of 6.0 °C. Furthermore, to improve the heat transfer performance between the water in the tank and fluids flowing through the tank in pipes, the inlets of high-temperature fluids from AW-HPs and WW-HPs are on the top of the tank, while the outlets are on the bottom of the tank. In addition, the inlets of low-temperature fluids from SH and VH networks and charged from the BTES loop are on the bottom of the tank, while the outlets are on the top of the tank.

As the local hybrid energy system is not designed totally self-sufficient, additional heat energy is also imported from the traditional DH network as a back-up. The auxiliary heater Type659 in TRNSYS was selected to model the DH network. Back-up heaters were prepared separately for each heating network (e.g., SH, VH and DHW), and were controlled based on the inlet temperature of fluids in the local energy system. Fig. 8 presents a simplified control logic for back-up heaters. If

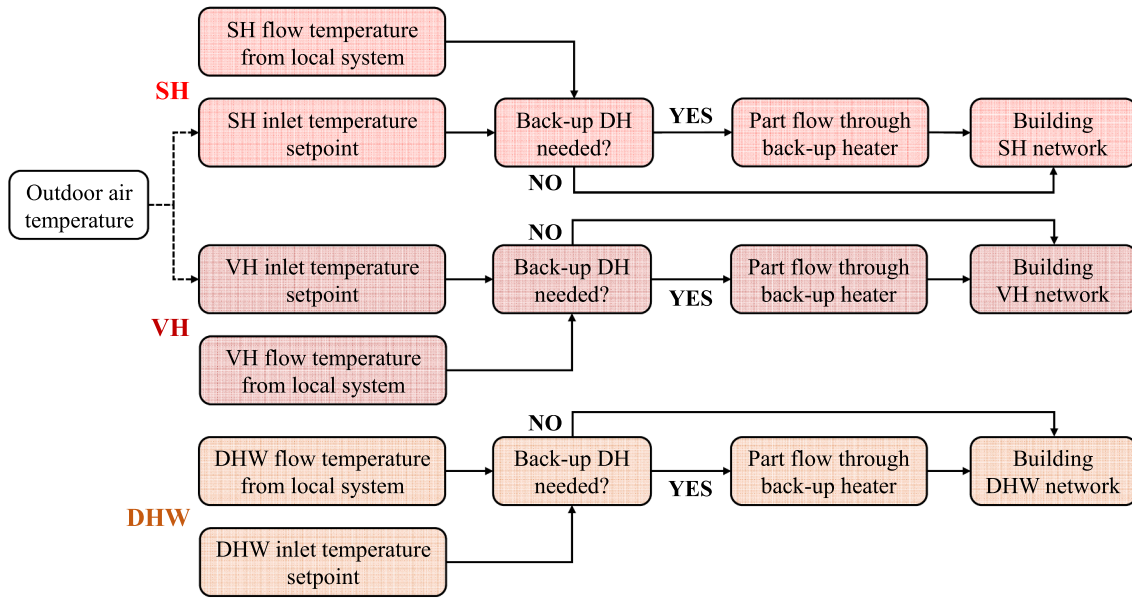


Fig. 8. Control logic for back-up heaters.

the incoming fluid temperature is lower than the set point of building heating network, the back-up heater is needed to heat the fluid to the set temperature. It is noted that, if all the heat-transfer fluid flows through the back-up heater, the temperature may increase too high. Thus, devices (e.g., flow diverters, mixing valves and temperature indicators) are applied to divide part of the fluid to flow through the back-up heater, and the rest to the mixing valve straightly, so that the set point temperature is met after mixing.

The core component of the cooling system is a 20 m³ cold buffer tank from which the water flows into the building cooling network at almost a constant temperature of 15 °C. The maximum outlet temperature from the SC network is 18 °C, while the flowrate is decided by the temperature difference and cooling demand. In summertime, cooling demand is supplied by WW-HPs using a cold buffer tank as the load side and a heat buffer tank as the source side. In wintertime, WW-HPs discharge the heat energy from the BTES to the heat buffer tank, further meeting building heating demand with BTES as the source side and heat buffer tank as the load side. In addition, the removed excess heat from cooling system can be stored and utilized in the local hybrid energy system.

2.3. System performance indexes

Some indexes have to be introduced to evaluate and optimize the system performance. From an economic perspective, the life cycle cost (LCC) and LCOE were introduced to evaluate the economic feasibility of the local hybrid energy system. From an environmental point of view, renewable energy fraction (REF), life cycle carbon emissions and the costs of emission allowances were considered to evaluate how friendly the system is to the environment.

2.3.1. Life cycle cost

LCC is an important index to estimate if the system is worth developing further. LCC consist of investment costs and operation costs in each year, and can be calculated by Eq. (1).

$$LCC = \sum_t [(C_{i,t} + C_{o,t}) \times (1 + r)^{-t}] \quad (1)$$

where, LCC is the life cycle cost of system, €; $C_{i,t}$ is the investment costs in year t , €; $C_{o,t}$ is the operation costs in year t , €; $(1 + r)^{-t}$ is the discount factor for year t , in which the interest rate is set as 3% referring to EU

recommendations for long-term investments [43] and t for initial year is 0.

Investment costs are assumed only in the initial year, and the detailed costs of system components are obtained from manufacturers, internet sources, and other related studies (Shown in Table 4). In addition, a value added tax (VAT) of 24% should be included in all investment costs.

Operation costs are defined by Eq. (2), including electricity costs and maintenance costs. Moreover, profit of surplus PV electricity sold to the grid is subtracted from the sum of operation costs.

$$C_{O,t} = \sum C_{e,import} - \sum C_{e,export} + C_{M,t} \quad (2)$$

where, $C_{e,import}$ is the hourly costs for electricity imported from the grid, €, calculated with Eq. (3); $C_{e,export}$ is the hourly surplus electricity selling profit, €; $C_{M,t}$ is the annual maintenance costs, €.

$$C_{e,import} = P_{e,buying} \times E_{e,import} \quad (3)$$

where, $P_{e,buying}$ is the hourly electricity buying price, €/MWh, calculated with Eq. (4); $E_{e,import}$ is the hourly imported electricity, MWh.

$$P_{e,buying} = (P_{Elspot} + P_{CF,buying} + P_{e,distribution} + P_{e,tax}) \times (1 + \frac{VAT}{100}) \quad (4)$$

where, P_{Elspot} is the hourly Nordpool Elspot price, €/MWh; $P_{CF,buying}$ is the commission fee for buying electricity, 3.0 €/MWh [51]; $P_{e,distribution}$ is the electricity distribution price, 31.4 €/MWh [52]; $P_{e,tax}$ is the electricity tax, 22.5 €/MWh [52]; VAT is the value added tax, 24%.

Considering the variation of electricity prices in different years,

Table 4
Costs for components of the local energy system.

Component	Cost	Unit	Reference
PV panel	1000	€/kW _p	[44]
AW-HP	410	€/kW	[45]
WW-HP	280	€/kW	[46]
Buffer tank	1570	€/m ³	[47]
Borehole drilling	38	€/m	[48]
BTES excavation	6	€/m ³	[41]
BTES insulation	75	€/m ³	[49]
Local pipes for heating	108	€/m	[50]
Local pipes for DHW	48	€/m	[50]

Nordpool Elspot prices, of five years from 2014 to 2018, were used in sequence to generate the electricity price profile for the whole calculation period of 25-years life cycle. In addition, the escalation rate of electricity price was assumed to be 1% conservatively.

Selling surplus PV electricity to the grid lowers the total operation costs, and the hourly surplus electricity selling profit can be calculated by Eq. (5).

$$C_{e,export} = P_{e,selling} \times E_{e,export} \quad (5)$$

where, $P_{e,selling}$ is the hourly electricity selling price, €/MWh, calculated with Eq. (6); $E_{e,export}$ is the hourly exported electricity, MWh.

$$P_{e,selling} = P_{Elspot} - P_{CF,selling} \quad (6)$$

where, $P_{CF,selling}$ is the commission fee for selling electricity to the grid, 2.4 €/MWh [53], subtracted from Nordpool Elspot price.

For simplicity, the annual maintenance cost was assumed to be 5% of total investment costs divided by the time of whole life cycle, as defined by Eq. (7).

$$C_{M,t} = \frac{0.05 \sum_t C_{I,t}}{T_{LC}} \quad (7)$$

where, $\sum_t C_{I,t}$ is the total investment costs of system, €; T_{LC} is the life cycle time (25 years) of the local hybrid energy system.

2.3.2. Levelized cost of energy

To further evaluate the system performance and compare its profitability with traditional DH, the cost of establishing one on-site heating energy system unit needs to be calculated. Thus, as defined by Eq. (8), LCOE is a more reasonable economic index than LCC. In this process, total costs and the amount of produced energy were calculated for each year. The costs were discounted and summed up for the whole life cycle, and finally divided by the total amount of produced energy discounted.

$$LCOE = \frac{LCC}{\sum_t [E_t \times (1+r)^{-t}]} = \frac{\sum_t [(C_{I,t} + C_{O,t}) \times (1+r)^{-t}]}{\sum_t [E_t \times (1+r)^{-t}]} \quad (8)$$

where, LCOE is the levelized cost of energy, €/MWh; E_t is the amount of heat energy produced, MWh.

2.3.3. Renewable energy fraction

Renewable energy fraction (REF) indicates the proportion of energy demand covered with energy produced by measures using renewable resources (e.g., PV panels). On-site heat energy fraction (OHEF) is needed to be introduced in Eq. (9) firstly before defining the REF.

$$OHEF = 1 - \frac{E_{DH,import}}{E_{demand}} \quad (9)$$

where, OHEF is the on-site heat energy fraction; $E_{DH,import}$ is the heat energy imported from DH grid, MWh; E_{demand} is the building total heating energy demand, MWh.

Considering the grid electricity is also imported in the hybrid energy system to operate WW-HPs, REF is defined differently from OHEF, taking grid electricity consumption into account (Shown in Eq. (10)).

$$REF = 1 - \frac{E_{grid,import} + E_{DH,import}}{E_{demand}} \quad (10)$$

where, REF is the renewable energy fraction; $E_{grid,import}$ is the electricity imported from the grid for HPs, MWh.

2.3.4. Carbon emissions

On-site stored heat energy reduces the heat supply from DH, and decreases CO₂ emissions as the electricity generated with PV panels is carbon-free. However, except of electricity from PV systems, the operation of HPs requires additional electricity from the grid, which

increases CO₂ emissions from power plants. Thus, the total carbon emission level should be evaluated in the local hybrid energy system to prove if the system is environmentally friendly.

Emission factor of 164 g/kWh is used for DH [54]. Emission factors for electricity production vary monthly between summer and winter times, which are summarized in Table 5.

If the capacity of DH plants is more than 20 MW, emission allowances should be considered with the aim to reduce carbon emissions [55]. The price of one emission allowance traded on the EU emissions trading system has increased during past few years [56], and has reached around 60 €/t [57]. This paper calculated the life cycle emission cost level of the system using a constant price value of 60 € per tonne emission allowance.

2.4. Optimization

This section describes the optimization of the system, and defines the objective functions, constraints, decision variables and the solution procedure.

2.4.1. Optimization definition

The system optimization goal is to find out the optimal solution with high performance and low costs. The optimization problem is defined by Eq. (10) with objective functions, constraints and decision variables, while objective functions are related to system performance and costs. The system performance optimization is for minimizing the amount of heat energy from DH grid and maximizing on-site energy production, while cost optimization is to minimize LCOE for the system profitability improvement. The optimization process is constrained by two factors, the maximum area of PV panels that can be installed, and the value of the decision variable must be within the lower and upper limits.

$$\begin{aligned} & \min \{f_{DH,import}(x), f_{LCOE}(x)\} \\ & \text{s.t.} \\ & A_{PV}(x) \leq 2100m^2 \\ & l_{i,min} \leq x_i \leq l_{i,max}, i \in \{1, \dots, 10\} \end{aligned} \quad (10)$$

where, $f_{DH,import}(x)$ is the amount of imported energy from DH, MWh; $f_{LCOE}(x)$ is the system levelized cost of energy, €/MWh; $A_{PV}(x)$ is the area that PV panels can be installed, m²; x_i is the decision variable introduced in Table 6; $l_{i,min}$ is the lower limit for decision variable x_i ; $l_{i,max}$ is the upper limit for decision variable x_i .

Decision variables affect the system performance significantly, and thus were selected to be optimized with reasonable limits for different components. Table 6 shows the decision variables relevant to the system design, including reasonable limits according to the use case. Limitations for geometric dimensions (e.g., the buffer tank volume, BTES volume and the height-to-width ratio of BTES) were decided based on the test simulation. Upper limit of PV capacity depends on the maximum amount of PV panels installed on the rooftops. The range for tilt angle of PV panels is wide as it might vary based on when the peak PV electricity demand may occur. Capacities for HPs are based on the number and nominal capacities for AW-HPs and WW-HPs. The range for borehole density can describe the distances between boreholes, which was set from 0.05 to 0.2 borehole/m² to reflect different effects on heat transfer performance. The maximum number of boreholes in a series was decided to be 4 according to Hirvonen and Sirén [41]. The minimum value set for BTES insulation thickness is 0 m as it might be infeasible to insulate the BTES in some situations, while the maximum one was set as 4 m, which is high enough to test whether higher insulation thickness is beneficial or not.

2.4.2. Optimization solution

The optimization problem is multi-objective as two objective functions were defined in this study. Multi-objective optimization (MOO),

Table 5
Monthly CO₂ emission factors of electricity production (g/kWh).

Month	Jan.	Feb.	Mar.	Apr.	May	Jun.	Jul.	Aug.	Sept.	Oct.	Nov.	Dec.
Factor	173	174	156	132	125	85	81	115	148	143	131	131

Table 6
Decision variables of the optimization problem.

Decision variable	Unit	Min	Max	Description
Buffer tank volume	m ³	20	200	Volume of warm buffer tank
PV capacity	kW	40	340	Nominal PV system total capacity
PV tilt angle	°	10	80	Tilt angle of PV panels
AW-HP capacity	kW	160	960	Total thermal power of AW-HPs
WW-HP capacity	kW	30	480	Total thermal power of WW-HPs
BTES volume	m ³	50,000	200,000	BTES total volume
BTES shape	–	0.25	4	Height-to-width ratio of BTES
Borehole density	borehole/m ²	0.05	0.2	Number of boreholes per m ²
Boreholes in series	–	1	4	Number of boreholes in series
BTES insulation thickness	m	0	4	BTES top insulation layer thickness

also known as Pareto optimization, is required to find out the Pareto-optimal solutions (namely the Pareto front). Genetic algorithm (GA), performing well in solving MOO problems, is developed based on evolution theory, where the fittest individuals survive and transfer their genetic information to the following generations [58]. Fig. 9(a) shows the main process of performing GA in optimization, which was realized via Multi-Objective Building Optimizer (MOBO) software developed by Aalto University and Technical Research Centre of Finland. Fig. 9(b) shows the process of combining optimization in MOBO and system simulation in TRNSYS using MATLAB as the media. The optimization starts with MOBO randomly, selecting initial decision variables based on the pre-defined limits. Decision variables are input to TRNSYS for performing system simulation for the 4-years period. After the simulation is

completed, MATLAB reads the simulation results from the TRNSYS output file and calculates the life cycle performance indexes of the system. The calculation results are printed to an output file and read by MOBO for creating mutations and crossovers in the population. In addition, MOBO selects the new decision variables based on the results of the previous generation, and the process is performed again similarly until the defined number of generations to be calculated is reached.

To make sure enough cases are computed, we set the maximum number of generations as the stopping criterion for optimization. The population size, meaning the number of cases that are simulated to form one generation, is set to 30. The number of generations, meaning how many populations are calculated, is 150. After altogether 4500 different cases were simulated, the Pareto front was formed based on the results of the last generation. The other two key indexes in GA are the mutation probability and crossover probability. If the mutation probability is too small, the ability of mutation operation to produce new individuals will be poor. If it is larger than 0.5, the mutations happen too often and the optimization will change to a random search. Thus, the mutation probability was set at 0.125 in this paper. If the crossover probability is too large, it will destroy the excellent structure formed in the population. However, a small crossover probability is too slow to discover new individuals. Thus, the crossover probability generally ranges from 0.4 to 0.99 and was set at 0.9 in this paper.

3. Results

3.1. Optimization results

Fig. 10 shows the multi-objective simulation result for each calculated case, where the Pareto front is formed from all the mathematically equal optimization results, which are presented by red points. The Pareto optimal solutions consist of 93 optimal results, of which the solution with the lowest imported district heat and highest LCOE is marked as number #1, and the solution with the lowest LCOE and highest

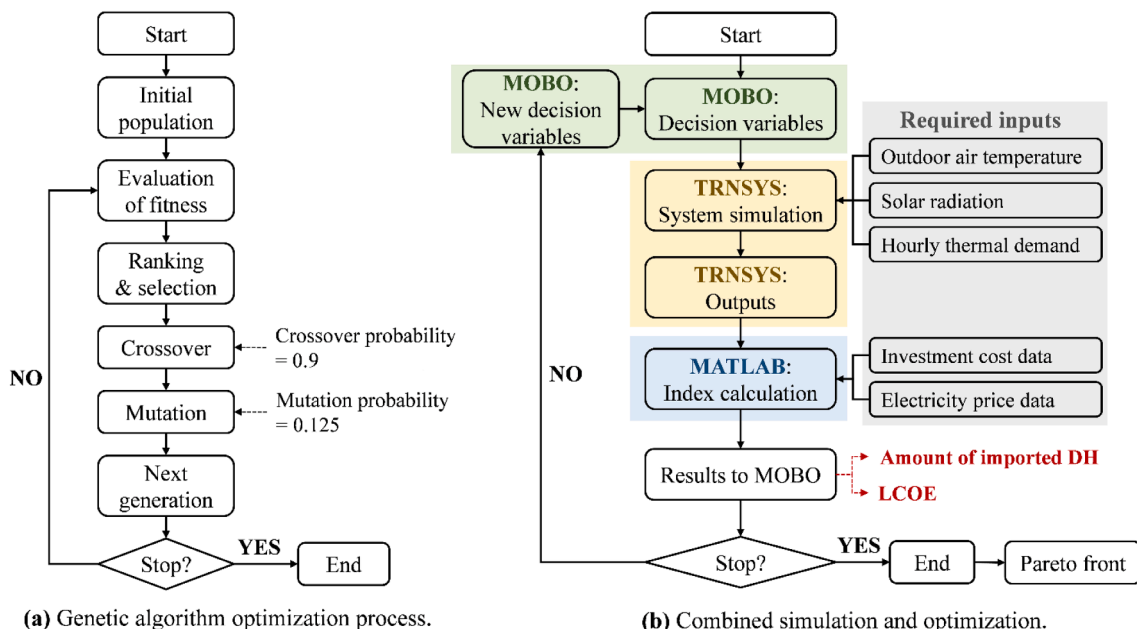


Fig. 9. Optimization process.

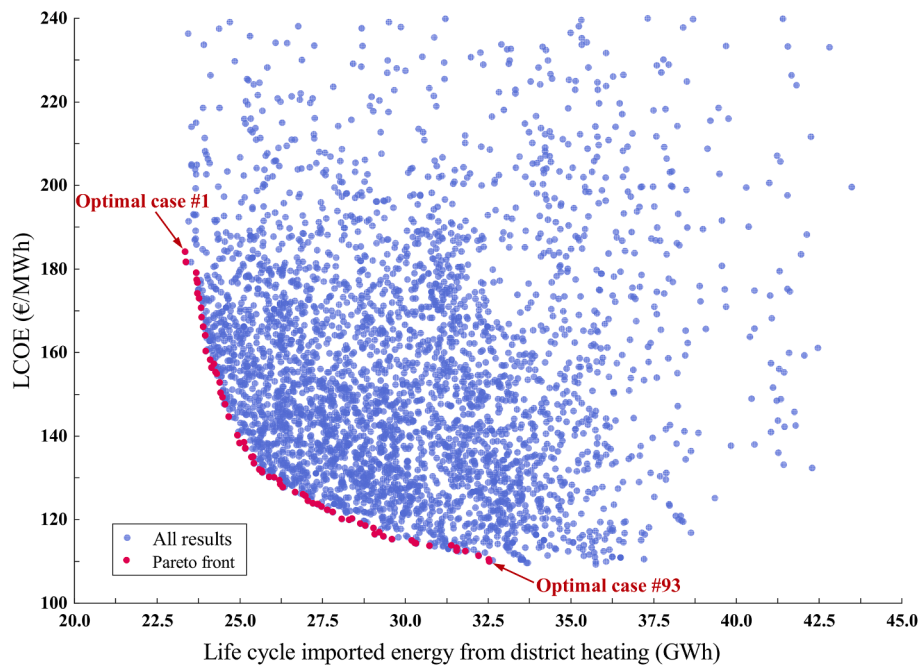


Fig. 10. The multi-objective simulation results and Pareto optimal solutions.

imported district heat is marked as number #93. None of the optimization results is dominating and further comparison is needed to find out more detailed differences between the optimal solutions.

Fig. 11 shows the LCC and REF performances of the 93 optimal solutions. The REF value increases as the LCC increases, which indicates that, with higher costs, the system can produce more on-site energy and lower the demand for off-site energy from DH and grid electricity. The main reason is that producing more on-site heat energy generally requires a higher investment cost for a larger system size and also a higher operation cost for the electricity used by heat pumps. In addition, by analysing the cost structure of different solutions, BTES has the biggest effect on the LCC, whose cost consists of several main components (e.g., Borehole drilling, excavation, and insulation costs). The main difference in the LCC of 93 solutions is caused by the difference in BTES size. In solutions with a larger investment in the BTES, the LCC increases significantly and more heat energy can be stored seasonally. Thus, more heating demand can be met by on-site energy, rather than the energy from district heating, which increases the REF. As for other components, the larger BTES requires more heat pumps (HPs) to produce the stored

heat energy, thus the investment costs and operation costs on HPs also increase, which further increases the LCC. The cost of PV system remains almost constant, indicating that the PV capacity keeps relatively the same for different solutions, which is the maximum limited by the available roof area.

Fig. 12 shows the life cycle heat energy distribution and LCOE values of the 93 optimal solutions. Solution #1 has the highest supplied on-site heat energy of 27.94 GWh and the highest LCOE of 184.11 €/MWh, while solution #93 has the lowest supplied on-site heat energy of 18.75 GWh and the lowest LCOE of 109.99 €/MWh. Applying the local hybrid energy system can achieve 54% DH reduction in the most expensive solution, and 37% DH reduction in the cheapest solution. In Fig. 11 and Fig. 12, the REF and on-site heat energy start to saturate while the LCOE rises faster. The reason is that the energy generation is limited by the PV capacity, which is always maxed out as there is no room to add more. Thus, increasing the size of the BTES system provides a less and less additional benefit, since no more renewable energy is being stored.

Life cycle PV electricity distribution of the 93 optimal solutions is shown in Fig. 13. In all solutions, AW-HPs consume the largest share of

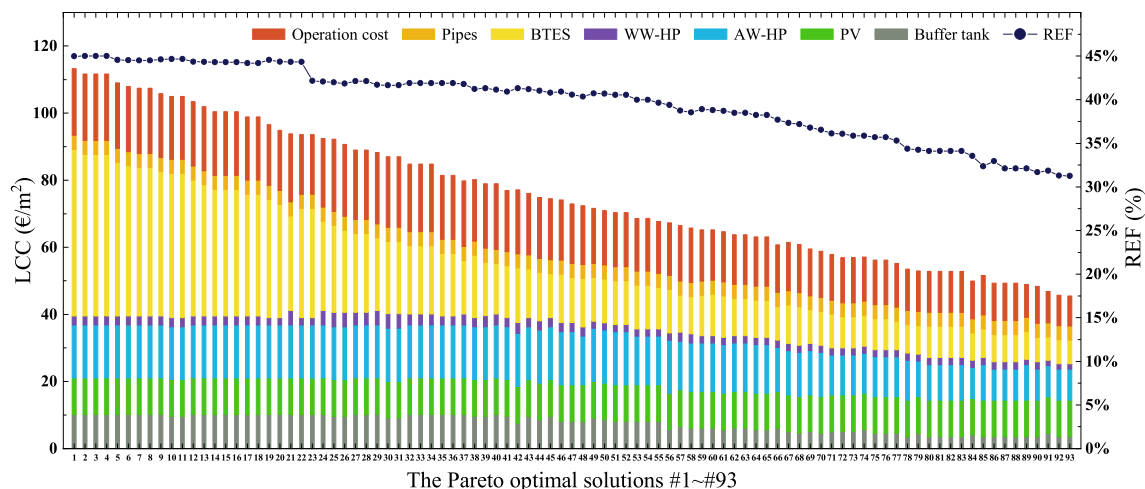


Fig. 11. LCC and REF performances for the 93 optimal solutions.

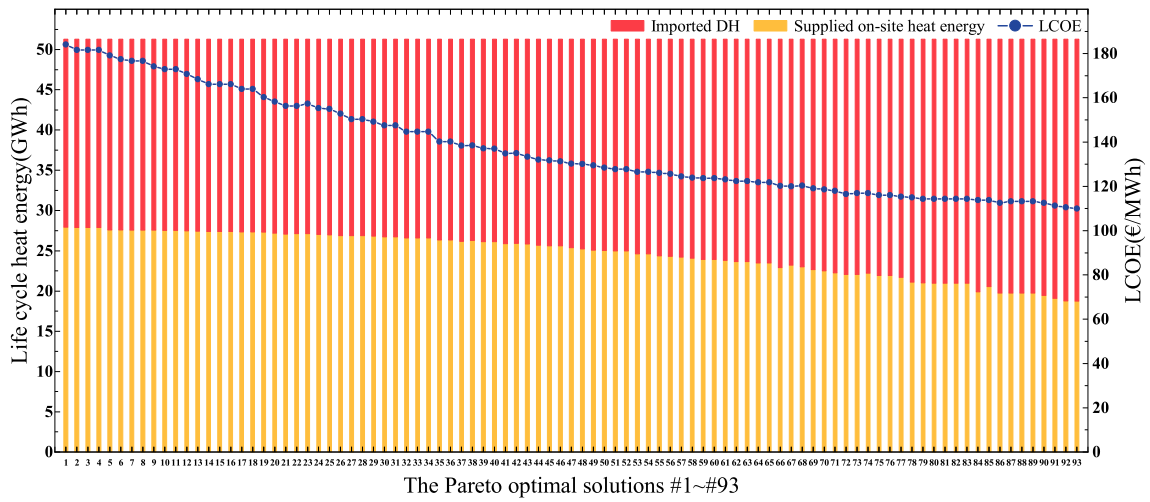


Fig. 12. Annual supplied on-site heat energy, imported district heat and LCOE.

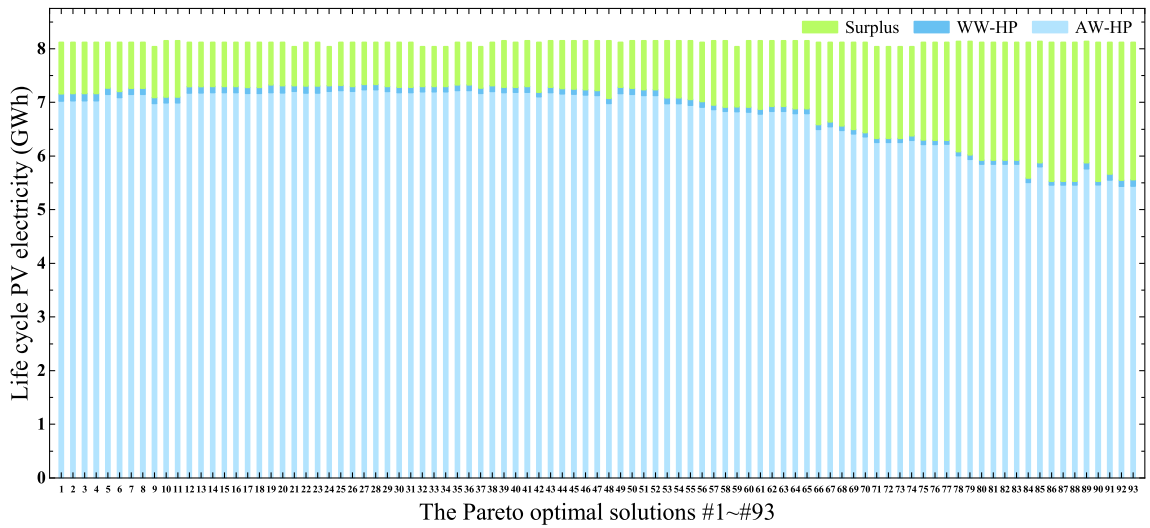


Fig. 13. Distribution of PV electricity.

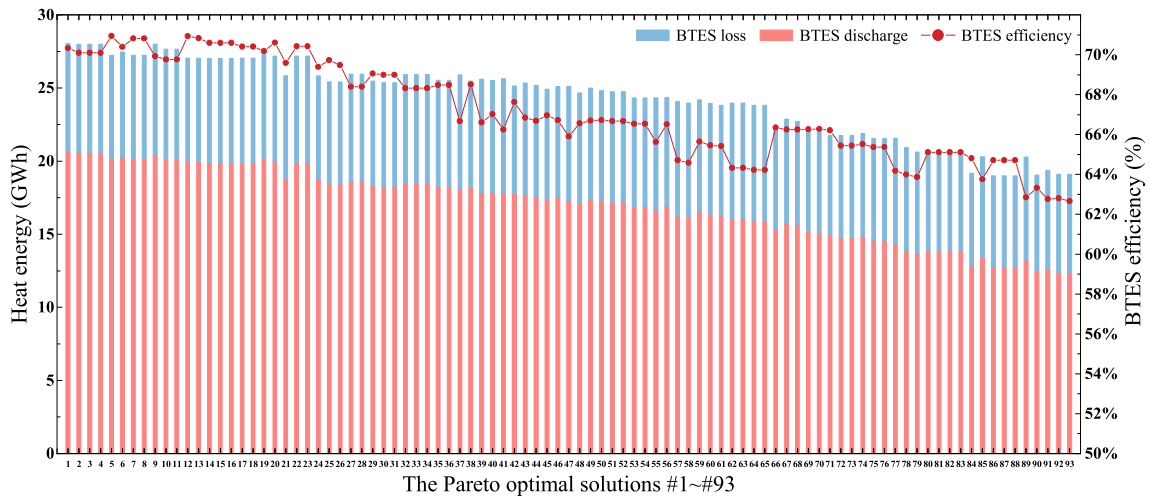


Fig. 14. Performance of seasonal storage BTES.

PV electricity, while WW-HPs consume a very small share. The reason is that WW-HPs operate mainly in wintertime when the generation of PV electricity is very low due to poor solar radiation. In each optimal solution with the same maximum PV capacity, the total amount of generated PV electricity varies slightly with different tilt angle (30°-45°) of PV panels. The share of surplus PV electricity is higher in solutions with lower LCOE, which indicates that the maximum capacity of PV panels is still worth investing in even if the system is small in scale. Although there is not enough electricity demand for HPs to consume all the generated PV electricity in a small system, the surplus PV electricity can be sold to the grid for economic benefits.

Fig. 14 presents the performance of BTES, which shows that cutting the investment for BTES lowers the system size, which decreases the capacity of seasonal storage. Thus, the annual amount of energy discharged from BTES also decreases. The efficiencies of BTES deviate between 63% and 70% in different cases, while the deviation could be caused by BTES temperature level, surface-to-volume ratio and insulation thickness.

3.2. Analysis for selected cases

As a multi-objective optimization problem, in total 93 solutions formed the Pareto front but they performed differently on the two objectives. For further analysis, four cases are selected from the 93 ones as marked on the Pareto front in Fig. 15. Considering extreme conditions, the solution, with the highest LCOE of 184 €/MWh and the largest amount of on-site produced heat energy, is selected as case #1; the solution with the lowest LCOE of 110 €/MWh is selected as case #4, whose share of total heating demand covered by on-site energy is the smallest of all the solutions. In addition, the solution, with roughly half of the total heating demand covered with on-site energy, is selected as case #2. And the solution whose LCOE is just below 120 €/MWh is selected to be the case #3, as a better one considering both economic and energy performance. Table 7 summarizes the system decision variables of these four cases in detail, while Table 8 summarizes their key indexes. As mentioned in Section 2.2.1, the system requires a heat-up time and has no significant change in the BTES temperature after a 4-year simulation, so the fourth year is chosen as the typical year for evaluating annual energy performance.

Table 7
System description for the selected cases.

System properties	Unit	Case #1	Case #2	Case #3	Case #4
Decision variable					
Buffer tank volume	m ³	200	190	10	70
PV capacity	kW	340	340	340	340
PV tilt angle	°	35	35	30	35
Total AW-HP capacity	kW	960	960	720	560
Total WW-HP capacity	kW	300	300	240	180
Detailed BTES properties					
BTES volume	m ³	130,000	90,000	60,000	50,000
BTES shape	–	1.00	1.25	1.25	1.50
Borehole density	borehole/m ²	0.150	0.075	0.075	0.075
Boreholes in series	–	3	1	1	1
BTES insulation thickness	m	2.75	1.50	0.25	0.00
Cross-sectional area	m ²	2370	1600	1220	960
BTES width	m	55	45	39	35
BTES height	m	55	56	49	52
Number of boreholes	–	355	120	91	72
Total flow of heat transfer fluid	kg/s	39.4	40.0	30.3	24.0

Table 8
Key indexes of the 4 selected cases.

Index	Unit	Case #1	Case #2	Case #3	Case #4
LCOE	€/MWh	184	138	116	110
Annual supplied on-site energy	MWh	1160	1086	912	768
Annual imported district heat energy	MWh	844	918	1092	1236
On-site Heat Energy Fraction (OHEF)	%	58	54	45	38
Renewable Energy Fraction (REF)	%	41	38	33	29

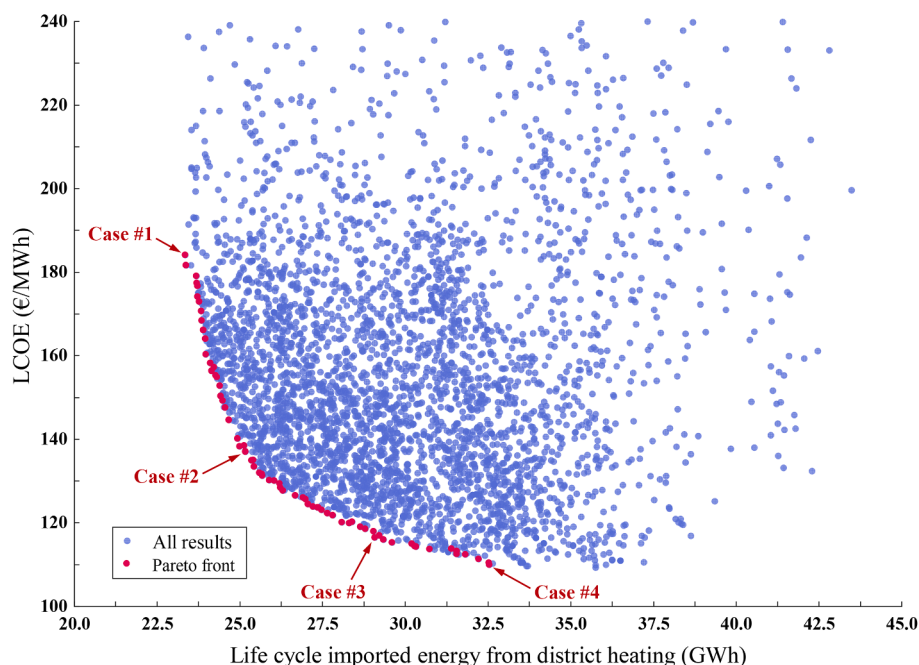


Fig. 15. Pareto front and four selected optimal solutions.

The increase in system capacity (e.g., buffer tank volume, BTES volume and the capacity of HPs) leads to the increase in the LCOE and the amount of supplied on-site heat energy. PV capacity remains maximum as it is limited by the fixed amount of roof area for PV system installation regardless of building height in multi-storey buildings. And the PV tilt angles are all quite low in the 4 cases to maximize the PV electricity generation in summertime.

Fig. 16(a) shows the LCC, REF and on-site heat energy fraction (OHEF) values of 4 cases. The investment cost of BTES in case #1 is significantly higher than in other cases, because case #1 has the largest seasonal storage size, the largest borehole density and the thickest insulation layer. REF and OHEF both increase with the system LCC increases, as a consequence of the increase in storage capacity. However, REF does not increase as rapidly as OHEF, for the reason that grid electricity consumed by WW-HPs is considered when calculating REF and the more on-site energy produced, the more electricity WW-HPs consume. Fig. 16(b) shows the LCOE values and annual heat energy distribution of each case. To further analyze heat distribution, heating demands of SH, VH and DHW are separated, while the analysis results are as follows. Firstly, a significant share of SH demand can be covered by on-site energy even with the lowest LCOE in case #4. In addition, over half of the DHW heating demand is covered by DH even with the highest LCOE in case #1. At last, the significant difference in LCOE between case #1 and case #2 only brings a very slight difference in on-site energy production, indicating that it would be infeasible to maximize the on-site energy production with the largest system size.

Fig. 17 shows the fluctuation of temperature level in BTES during the simulation period for each case. From the 1st year of operation, the BTES starts to heat up from the initial temperature of 6.0 °C (average ground temperature), and thus the overall temperature level in the first year is significantly lower than that in later years. There is still a slight difference between the temperature level in the second and third years. However, the BTES temperature becomes constant from the 4th year, which proves the system operates in a relatively stable status. Considering the control logic in Section 2.2.3, the seasonal storage ceases discharging heat when the tank temperature reaches the lower limit of 12 °C. Comparing the temperature curves, it is concluded that the larger the BTES volume, the lower the maximum temperature level, which also can explain to some degrees why the BTES efficiency of larger storage is better than smaller ones.

3.3. Optional control scenarios

Solar radiation is unavailable during some periods (e.g., night times in summer), which means no PV electricity can be used to drive the AW-HPs at these times. Instead, grid electricity can be imported for AW-HPs operation under the circumstance of no PV electricity. According to this, two different AW-HP control strategies were proposed and simulated for

the cases. In all control scenarios, it is prioritized to utilize PV electricity for AW-HPs, but if PV electricity is not available, AW-HPs can be driven by grid electricity and controlled based on outdoor air temperature.

According to the data provided by the manufacturer [45], the COP of AW-HP NIBE F2120-20 is relatively high when the outdoor air temperature is above 5 °C and is high enough especially when the temperature reaches 15 °C. Thus, we chose 5 °C and 15 °C as the two critical points to design the optional control strategies. Table 9 summarizes the scenarios for different control strategies. Number 1–4 still represents these four cases. Letter A-D represents the scenarios with different control strategies for AW-HPs. Scenario A is the original solution with no changes. In scenario B, AW-HPs operate with grid electricity when PV electricity is not available and outdoor air temperature exceeds 15 °C. In scenario C, AW-HPs operate with grid electricity when PV electricity is not available and outdoor air temperature exceeds 5 °C. In scenario 1A, the largest system capacity can produce almost the maximum possible amount of on-site heat energy, but there is not enough heating demand to utilize that energy in the discharge period. To increase the utilization rate of on-site heat energy, control scenario D is developed for case #1. Among all the control scenarios, DHW is heated up by DH in summer to maximize the charging potential of BTES. However, in scenario 1D, DHW is pre-heated with on-site heat energy all year round instead of being heated totally with DH in summertime.

Fig. 18 shows the simulation results for the 13 different control scenarios, and Fig. 18 (a) shows the values of LCC, REF and OHEF. Assuming that no additional investment is needed for different control strategies, the total investment costs in the same case with different scenarios are the same. However, the operation costs increase due to the increase in grid electricity use. In general, the OHEF is increased in both control scenarios B and C, where AW-HPs can produce more heat energy. The increase is more significant in cases #3 and #4 whose systems are smaller in scales than cases #1 and #2, indicating that the strategy of using additional grid electricity to drive AW-HPs is more beneficial in small systems. In the control scenario 1D, OHEF and REF are improved drastically with additional utilization of on-site heat energy to pre-heat the DHW. The share of on-site heat energy increases to nearly 90% of the total heating demand, while REF does not increase that much because more grid electricity is imported.

LCOE and annual heat energy distribution are shown in Fig. 18(b). In cases #2, #3 and #4 with grid electricity imported for AW-HPs, the share of on-site heat energy increases but LCOE changes slightly. In addition, despite the additional utilization of grid electricity to charge the seasonal storage, the share of on-site heat energy seems to be the same in scenarios 1A, 1B and 1C. The reason is that all the SH and VH demand in winter is possible to be covered with on-site heat energy, and there is no need to charge more energy to BTES, which also explains why the improvement of DHW control is needed. As DHW is pre-heated with on-site heat energy instead of being heated totally with DH in scenario

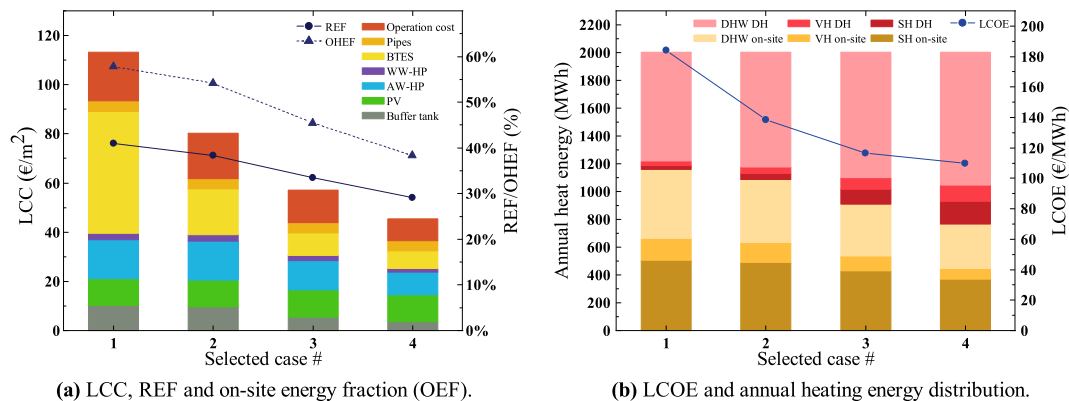


Fig. 16. Performance of the 4 selected cases.

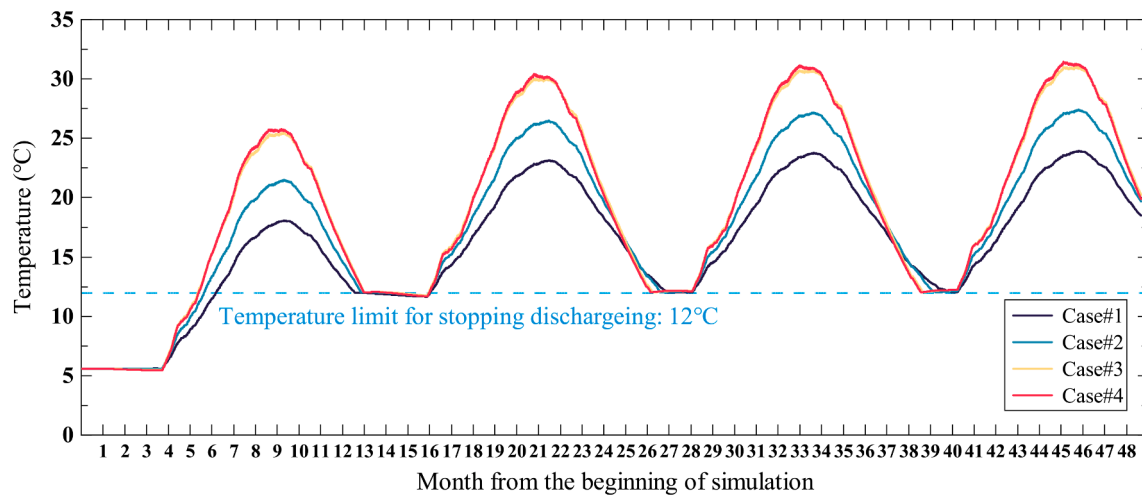


Fig. 17. BTES temperature improvement during the simulation period.

Table 9
Description of different control scenarios.

	Scenario			
	1. Highest LCOE	2. On-site heat covers half of the demand	3. LCOE below 120 €/MWh	4. Lowest LCOE
A: AW-HP uses only PV	1A	2A	3A	4A
B: AW-HP operates with grid-electricity when outdoor temperature is above 15 °C	1B	2B	3B	4B
C: AW-HP operates with grid electricity when outdoor temperature is above 5 °C	1C	2C	3C	4C
D: AW-HP operates with grid electricity when outdoor temperature is above 5 °C and DHW preheated with on-site heat all year round	1D			

1D, the share of on-site heat energy increases and the LCOE drops down drastically.

Fig. 18(c) shows the annual performance of BTES for different scenarios. The efficiency decreases significantly in cases #1 and #2 because the heat loss from BTES increases due to the relatively higher temperature level. Another reason why the efficiency decreases in case #1 is that the additional heat energy charged to the storage cannot be fully utilized as there is not enough heating demand during the discharge period. Even though the different DHW control strategy in scenario 1D is implemented, the amount of discharged heat energy does not increase significantly, which indicates that, in summertime, the DHW is preheated with the heat energy in the buffer tank rather than in BTES. Fig. 18(d) shows the annual temperature variation of BTES. In cases #1 and #2, the temperature limit for discharging of 12 °C is no longer reached when additional grid electricity is imported to charge more heat energy to BTES. It means that the seasonal storage might be charged overmuch unnecessarily as the demand for on-site heat energy is already fulfilled, but there is still discharging potential left. In most scenarios of cases #3 and #4, the temperature limit is still reached even though extra heat energy is charged to BTES using grid electricity. It indicates that all the heat energy in BTES is possible to be discharged and there is still potential to improve the utilization rate of on-site energy by charging more energy to the seasonal storage.

The annual distribution of consumed electricity is shown in Fig. 18 (e). PV electricity used by AW-HPs decreases when grid electricity is imported for AW-HPs. The reason is that the tank may be firstly charged with AW-HPs driven by grid electricity when the outdoor air temperature is suitable. After some time, the tank temperature has already reached high enough, thus there is no need to operate AW-HPs even though PV electricity is available. In scenario B, the increase of grid electricity utilized by AW-HPs is slight because the grid-drive time is shorter due to the higher air temperature required (15 °C) in the control strategy. The increase is more significant in scenario C with longer grid-drive time because the lower air temperature (5 °C) is required. The use of grid electricity for running WW-HPs decreased from scenario A to C in case #1. This is mainly because the maximum temperature level of BTES is higher with more heat energy charged, and increases the COP of WW-HPs. As for cases #2, #3 and #4, the more AW-HPs operate to charge the seasonal storage, the more WW-HPs operate as there is more heat energy in BTES to be discharged, which increases the grid electricity consumption of WW-HPs.

Fig. 18(f) shows the life cycle CO₂ emissions and emission costs for different scenarios, and separately presents the CO₂ emissions caused by DH and grid electricity use. Compared with the reference scenario in which total heating demand is covered with DH, all the solutions with hybrid energy systems succeed in lower CO₂ emissions due to the utilization of PV panels and HPs. Life cycle emission cost varies moderately between scenarios but changes significantly depending on the emission allowance price. From the perspective of emission reduction, it is not recommended in all cases to import grid electricity to operate AW-HPs, as the life cycle CO₂ emissions may decrease very slightly or even increase in some scenarios. Scenario 1D is an exception, where the total amount of CO₂ emissions decreases significantly mainly because the imported DH is reduced drastically as DHW is pre-headed with on-site heat energy all year round.

Table 10 summarizes the results of annual CO₂ emissions, carbon reduction rates and equivalent emission factors of on-site produced heat energy. Compared with the reference scenario, CO₂ emissions can be annually decreased by 100–150 tons in most optimal scenarios, while in the bolded optimal scenario 1D can be decreased even by 217 tons, achieving a maximum carbon reduction rate of 66%. The equivalent emission factor of on-site produced heat energy is significantly lower than that of DH or electricity grids. If the electricity from the grid is generated by wind and solar energy, the on-site energy production would be almost carbon-free.

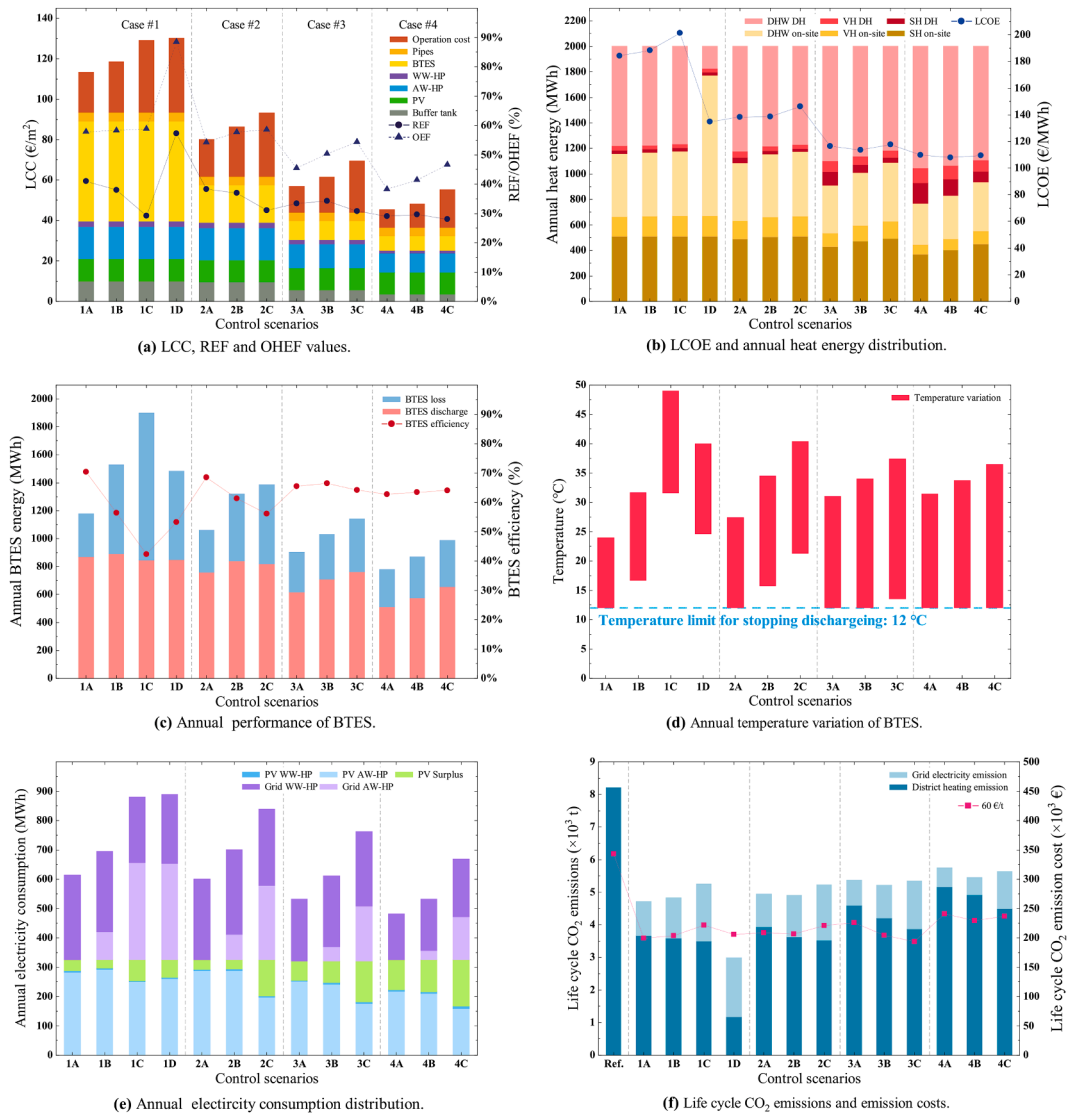


Fig. 18. Simulation results for different control scenarios.

Table 10

The annual CO₂ emissions, carbon reduction rates and equivalent emission factors of on-site heat generation.

Scenario	CO ₂ emissions of DH (t)	CO ₂ emissions of grid electricity (t)	Total CO ₂ emissions (t)	Carbon reduction (t)	Carbon reduction rates (%)	Equivalent emission factors (g/kWh)
Ref.	329	0	329	0	–	–
1A	138	44	183	146	44	38
1B	137	51	188	141	43	44
1C	135	70	205	124	38	59
1D	40	72	112	217	66	41
2A	151	42	193	136	41	39
2B	139	53	192	137	42	45
2C	136	69	205	124	38	58
3A	179	32	211	118	36	35
3B	163	41	205	124	38	41
3C	150	60	210	119	36	55
4A	203	24	227	102	31	31
4B	193	22	215	114	35	26
4C	175	47	222	107	33	50

4. Discussion

4.1. General analysis of the system

The studied local hybrid energy system is a potential solution to provide on-site heat energy for the residential district, and decentralizes heat energy production for CO₂ emission reduction. In solutions with a smaller system scale (e.g., cases #3 and #4), on-site produced energy was possible to cover 38–45% of total heating demand, and could reduce CO₂ emissions by 33–36% with REF of 29–33% and LCOE of 110–116 €/MWh. In solutions with a larger system scale (e.g., cases #1 and #2), 54–58% of total heating demand could be covered by on-site produced energy, and 41–44% of CO₂ emissions could be reduced with REF of 38–41% and LCOE of 138–184 €/MWh. Among all the selected cases, cases #2, #3 and #4 were more feasible to develop further, while Case #1 might be infeasible as the LCOE was significantly higher with no notable effect on REF improvement or CO₂ emission reduction.

By assuming the average values of AW-HP COP and BTES efficiency, a rule of thumb can be defined to estimate the local heat energy production based on PV capacity. PV panels with a nominal capacity of 100 kW can generate 95 MWh of electricity on an annual level. With PV electricity input, AW-HPs can operate with an average COP of 4.5 and produce 430 MWh of heat energy all charged into BTES. The average efficiency of BTES is assumed to be 60%, and approximate 260 MWh of heat energy can be discharged from BTES to the local heating network. Thus, it is roughly estimated that, 2.6 MWh of heat energy can be produced with a PV capacity of 1 kW in the local hybrid energy system. Applying this thumb rule, a total PV capacity of 770 kW is required to cover all the heating demand of the residential district.

Hirvonen and Sirén [41] have studied a fully electrified solar community in detached houses in Espoo, Finland. The results of the studied local hybrid energy system are compared with that in Hirvonen and Sirén's research. The nominal PV capacity is maximum reaching 0.01 kW/m² (scaled to the total floor area) in this research, while that ranges from 0.06 kW/m² to 0.1 kW/m² for most of their cases in Hirvonen and Sirén's research, which shows a significant difference. The expectation can be supported by the result comparison between this research and Hirvonen and Sirén's that it is the limited rooftop area that mostly restricts achieving an almost fully self-sufficient local energy system based on PV electricity. Thus, it can be concluded that limited PV capacity is the main reason, causing the solar energy fraction in the proposed local hybrid energy system is significantly lower than that in a fully electrified solar community composed of detached houses.

4.2. Limitation and further study

This paper mainly focuses on the pre-feasibility analysis of the proposed local hybrid energy system for the residential district. Further studies should be done to find out the more feasibility cost structure and operation strategy if the system is implemented in an actual residential district.

The energy demand profile is simulated in IDA ICE based on the apartment buildings modelled with current requirements of the Finnish Building Code. However, the actual building energy demand varies, depending on many uncertain factors (e.g., occupant behaviour). Therefore, more validation of the energy demand profile must be done to avoid unreasonable system scale when it is actually implemented.

In addition, this paper does not consider the demand response and optimal control system for the local hybrid energy system. Due to the lack of control algorithms base on weather forecasting and solar radiation prediction, importing grid electricity to produce more heat energy with AW-HPs decreases the utilization of PV electricity in many cases. It suggests that the optimization of system operation with demand response and suitable control algorithm is meaningful and would be a separate topic in the next study phase.

Considering the practical situation, it is more feasible to implement

the local hybrid energy system in a newly-designed neighbourhood than in existing neighbourhoods. The reason is that the heating networks in existing buildings usually operate with relatively higher temperatures than the assumed underfloor heating, which may decrease the efficiency of the local hybrid energy system. It is also worth noticing that, the studied local hybrid energy system requires more installation space for components such as BTES and buffer tank than the DH system. Pre-designing related to the layout of the site is necessary when the system is implemented, to locate the components to the site in a suitable way.

5. Conclusions

The building sector in the Nordic region covers a large share of energy consumption due to the cold climate and relatively higher heating demand. The utilization of renewable energy sources for heat energy production is a significant approach to reducing CO₂ emissions and mitigating climate change. Solar energy is a superior renewable energy source, while the main challenge in utilizing solar energy for heating is the seasonal mismatch of solar radiation and building heating demand. Decentralized heat energy production at neighbourhood level makes it possible for STES. A local hybrid energy system integrating PV power generation and STES is proposed and studied in this paper. When the amount of solar radiation is at the highest level in summer, heat energy produced by PV electricity is charged, and then discharged in winter when there is high building heating demand. The studied system is designed to cover part of the heating demand of a residential neighbourhood with 14 apartments. Multi-objective optimization is performed with system simulations and genetic algorithms, and the feasibility of the system is evaluated based on optimization results.

Based on cases with different system scales, 38–58% of the heating demand is covered by on-site produced heat energy with the LCOE of 110–184 €/MWh. If grid electricity is also imported for AW-HPs operation rather than only with PV electricity, 41–88% of the heating energy can be produced on site with the LCOE of 108–201 €/MWh. CO₂ emissions reduction of 102–217 tons is achieved annually in this system compared with the situation where all the heating demand is covered with DH.

As the on-site energy is produced based on PV electricity generation, the available rooftop area becomes the main limit for improvement of the system performance. If larger PV power stations (on external structures or vertically on the walls) can be utilized to produce heat energy, REF can be higher and the system might be more feasible. With moderate heat losses, BTES can be considered a high-efficiency seasonal storage system in this kind of residential neighbourhood. However, it is also the main economic component of the system. When the system is implemented on the site, the most important things are detailed ground investigations and precise pre-design for BTES.

Larger investments do not always increase the share of DH replaced with on-site renewable energy. However, with the purpose to decentralize heat energy production and reduce CO₂ emissions, system scales with high LCOE are worth developing further.

CRediT authorship contribution statement

Xiaolei Yuan: Methodology, Formal analysis, Writing – original draft. **Lassi Heikari:** Software, Data curation, Formal analysis. **Janne Hirvonen:** Conceptualization, Methodology, Supervision, Writing – review & editing. **Yumin Liang:** Writing – review & editing. **Markku Virtanen:** Supervision, Project administration. **Risto Kosonen:** Writing – review & editing, Supervision. **Yiqun Pan:** Writing – review & editing, Funding acquisition, Supervision.

Declaration of Competing Interest

The authors declare that they have no known competing financial

interests or personal relationships that could have appeared to influence the work reported in this paper.

Data availability

The authors are unable or have chosen not to specify which data has been used.

Acknowledgements

This paper has received funding from the National Natural Science Foundation of China (Grant No. 51978481).

References

- Nguyen KH, Kakinaka M. Renewable energy consumption, carbon emissions, and development stages: Some evidence from panel cointegration analysis. *Renewable Energy* 2019;132:1049–57. <https://doi.org/10.1016/j.renene.2018.08.069>.
- Adekoya OB, Olabode JK, Rafi SK. Renewable energy consumption, carbon emissions and human development: empirical comparison of the trajectories of world regions. *Renewable Energy* 2021;179:1836–48. <https://doi.org/10.1016/j.renene.2021.08.019>.
- Lindsey R. Climate Change: Atmospheric Carbon Dioxide. <https://www.climate.gov/news-features/understanding-climate/climate-change-atmospheric-carbon-dioxide>; 2020 [accessed December 2021].
- IEA. Tracking Buildings 2020. <https://www.iea.org/reports/tracking-buildings-2020>; 2020 [accessed December 2021].
- IEA. Tracking Buildings 2021. <https://www.iea.org/reports/tracking-buildings-2021>; 2021 [accessed December 2021].
- Rohde D, Andresen T, Nord N. Analysis of an integrated heating and cooling system for a building complex with focus on long-term thermal storage. *Appl Therm Eng* 2018;145:791–803. <https://doi.org/10.1016/j.applthermaleng.2018.09.044>.
- Belaïd F, Zrelli MH. Renewable and non-renewable electricity consumption, environmental degradation and economic development: evidence from Mediterranean countries. *Energy Policy* 2019;133. <https://doi.org/10.1016/j.enpol.2019.110929>.
- García-Menéndez D, Ríos-Fernández JC, Blanco-Marigorta AM, Suárez-López MJ. Dynamic simulation and exergetic analysis of a solar thermal collector installation. *Alexandria Eng J* 2022;61(2):1665–77. <https://doi.org/10.1016/j.aej.2021.06.075>.
- Kong J, Lyu Y. Research on the development of photovoltaic industry based on A company. *Energy Rep* 2021;7:867–72. <https://doi.org/10.1016/j.egy.2021.09.187>.
- Ajiwiguna TA, Lee G-R, Lim B-J, Cho S-H, Park C-D. Optimization of battery-less PV-RO system with seasonal water storage tank. *Desalination* 2021;503. <https://doi.org/10.1016/j.desal.2021.114934>.
- Bahrami A, Okoye CO, Atikol U. The effect of latitude on the performance of different solar trackers in Europe and Africa. *Appl Energy* 2016;177:896–906. <https://doi.org/10.1016/j.apenergy.2016.05.103>.
- Chwieduk D. Impact of solar energy on the energy balance of attic rooms in high latitude countries. *Appl Therm Eng* 2018;136:548–59. <https://doi.org/10.1016/j.applthermaleng.2018.03.011>.
- E-hub. The Energy Hub Challenge. <https://www.e-hub.org/energy-hub-challenge.html>; 2018 [accessed December 2021].
- Yang T, Liu W, Kramer GJ, Sun Q. Seasonal thermal energy storage: a technological literature review. *Renew Sustain Energy Rev* 2021;139. <https://doi.org/10.1016/j.rser.2021.110732>.
- Salvestroni M, Pierucci G, Pourreza A, Fagioli F, Taddei F, Messeri M, et al. Design of a solar district heating system with seasonal storage in Italy. *Appl Therm Eng* 2021;197. <https://doi.org/10.1016/j.applthermaleng.2021.117438>.
- Mahon H, O'connor D, Friedrich D, Hughes B. A review of thermal energy storage technologies for seasonal loops. *Energy* 2022;239. <https://doi.org/10.1016/j.energy.2021.122207>.
- Novo AV, Bayon JR, Castro-Fresno D, Rodriguez-Hernandez J. Review of seasonal heat storage in large basins: Water tanks and gravel–water pits. *Appl Energy* 2010; 87(2):390–7. <https://doi.org/10.1016/j.apenergy.2009.06.033>.
- Babaei M, Nick HM. Performance of low-enthalpy geothermal systems: Interplay of spatially correlated heterogeneity and well-doublet spacings. *Appl Energy* 2019; 253. <https://doi.org/10.1016/j.apenergy.2019.113569>.
- Lim HS, Ok J, Park JS, Lee SJ, Karng SW, Kang YT. Efficiency improvement of energy storage and release by the inlet position control for seasonal thermal energy storage. *Int J Heat Mass Transf* 2020;151. <https://doi.org/10.1016/j.ijheatmasstransfer.2020.119435>.
- Cheruy F, Dufresne JL, Ait Mesbah S, Grandpeix JY, Wang F. Role of Soil thermal inertia in surface temperature and soil moisture-temperature feedback. *J Adv Model Earth Syst* 2017;9(8):2906–19. <https://doi.org/10.1002/2017ms001036>.
- Del Amo A, Martínez-Gracia A, Pintanel T, Bayod-Rújula AA, Torné S. Analysis and optimization of a heat pump system coupled to an installation of PVT panels and a seasonal storage tank on an educational building. *Energy Build* 2020;226. <https://doi.org/10.1016/j.enbuild.2020.110373>.
- Beausoleil-Morrison I, Kemery B, Wills AD, Meister C. Design and simulated performance of a solar-thermal system employing seasonal storage for providing the majority of space heating and domestic hot water heating needs to a single-family house in a cold climate. *Sol Energy* 2019;191:57–69. <https://doi.org/10.1016/j.solener.2019.08.034>.
- Kubiński K, Szablowski Ł. Dynamic model of solar heating plant with seasonal thermal energy storage. *Renewable Energy* 2020;145:2025–33. <https://doi.org/10.1016/j.renene.2019.07.120>.
- Schach R, Wollstein-Lehmkuhl AE. Decentralized heat supply with seasonal heat storage systems Comparison of different heating systems. *Energy Procedia* 2018; 155:320–8. <https://doi.org/10.1016/j.egypro.2018.11.046>.
- Saloux E, Candanedo JA. Model-based predictive control to minimize primary energy use in a solar district heating system with seasonal thermal energy storage. *Appl Energy* 2021;291. <https://doi.org/10.1016/j.apenergy.2021.116840>.
- Mi P, Zhang J, Han Y, Guo X. Study on energy efficiency and economic performance of district heating system of energy saving reconstruction with photovoltaic thermal heat pump. *Energy Convers Manage* 2021;247. <https://doi.org/10.1016/j.enconman.2021.114677>.
- Gabrielli P, Acquilino A, Siri S, Bracco S, Sansavini G, Mazzotti M. Optimization of low-carbon multi-energy systems with seasonal geothermal energy storage: The Energy Grid of ETH Zurich. *Energy Convers Manage* X 2020;8. <https://doi.org/10.1016/j.ecmx.2020.100052>.
- Raluy RG, Guillén-Lambea S, Serra LM, Guadalfajara M, Lozano MA. Environmental assessment of central solar heating plants with seasonal storage located in Spain. *J Cleaner Prod* 2021;314. <https://doi.org/10.1016/j.jclepro.2021.128078>.
- Maximov SA, Mehmood S, Friedrich D. Multi-objective optimisation of a solar district heating network with seasonal storage for conditions in cities of southern Chile. *Sustain Cities Soc* 2021;73. <https://doi.org/10.1016/j.scs.2021.103087>.
- Yuan XL, Lindroos L, Jokisalo J, Kosonen R, Pan YQ, Jin H. Demand response potential of district heating in a swimming hall in Finland. *Energy Build* 2021;248: 111149. <https://doi.org/10.1016/j.enbuild.2021.111149>.
- Yuan XL, Lindroos L, Jokisalo J, Kosonen R, Pan YQ. Study on waste heat recoveries and energy saving in combined energy system of ice and swimming halls in Finland. *Energy Build* 2021;231:110620.
- Ministry of the Environment. The National Building Code of Finland. <https://ym.fi/en/the-national-building-code-of-finland/>; 2019 [accessed December 2021].
- Ministry of the Environment. Decree of the Ministry of the Environment on the Energy Performance of New Buildings. <https://www.ym.fi/download/noname/%7BE12CDE2C-9C2B-4B84-8C81-851349E2880B%7D/140297>; 2009 [accessed December 2021].
- Espoo Esbo. Map service. <https://kartat.espool.fi/IMS/en/Map>; 2019 [accessed December 2021].
- Pearsall NM. Introduction to photovoltaic system performance. The Performance of Photovoltaic (PV) Systems 2017;1–19. <https://doi.org/10.1016/B978-1-78242-336-2.00001-X>.
- NREL. Photovoltaic Degradation Rates – An Analytical Review Preprint. <https://www.nrel.gov/docs/fy12osti/51664.pdf>; 2012 [accessed December 2021].
- GTK. Geological Survey of Finland, Annual review 2019. https://view.creator.taiqa.com/sites/all/files/public_files/documents/gtk/a457149911848212ce4e1621bb7693b8/document.pdf; 2019 [accessed December 2021].
- Engineering Toolbox. Solids, Liquids and Gases - Thermal Conductivities. https://www.engineeringtoolbox.com/thermal-conductivity-d_429.html; 2018 [accessed December 2021].
- Smolczyk U. Geotechnical Engineering Handbook Volume 2: Procedures. ISBN 978-3433014509; 2003.
- Hakala P, Huusko A, Leppäharju N, Martinkauppi I, Leppäharju N, Korhonen K. Evaluation of the Distributed Thermal Response Test (DTRT) Nupurinkartano as a case study. Report of Investigation 211. Geological Survey of Finland, Espoo, Finland; 2014.
- Hirvonen J, Sirén K. A novel fully electrified solar heating system with a high renewable fraction-Optimal designs for a high latitude community. *Renewable Energy* 2018;127:298–309. <https://doi.org/10.1016/j.renene.2018.04.028>.
- Engineering Toolbox. Ethylene Glycol Heat-Transfer Fluid Properties. https://www.engineeringtoolbox.com/ethylene-glycol-d_146.html; 2019 [accessed December 2021].
- European Commission. Commission Delegated Regulation (EU) of 16.1.2012. <http://edz.bib.uni-mannheim.de/edz/pdf/k/k-2011-10050-en.pdf>; 2012 [accessed December 2021].
- Photovoltaic electricity home. Offerings. <https://aurinkosahkoakoti.fi/tarjoukset/>; 2019 [accessed December 2021].
- NIBE. Products for larger properties NIBE F2120. https://www.nibe.eu/en-eu/products/products-for-larger-properties/NIBE-F2120_-34; 2019 [accessed December 2021].
- NIBE. Ground source heat pumps NIBE F1345. https://www.nibe.eu/en-gb/products/heat-pumps/ground-source-heat-pumps/NIBE-F1345_-32; 2019 [accessed December 2021].
- IEA. Technology and demonstrators-Technical Report Subtask C - Part C1: Classification and benchmarking of solar thermal systems in urban environments. IEA-SHC-Task52-STC1-Classification-and-benchmarking-Report-2016-03-31.pdf; 2016 [accessed December 2021].
- Techeat. Porakaivo. <http://www.techeat.fi/porakaivo-yleisimmat-kysymykset/>; 2018 [accessed December 2021].
- K-rauta. Thermisol insulation panel. <https://www.k-rauta.fi/rautakauppa/eristy-slevy-thermisol-eps-120-routa-50x1000x1200mm-12m2>; 2019 [accessed December 2021].

- [50] Rauheat. PexFlex Plus local heating pipe. https://www.rauheat.fi/weboost.php?si_vu=tiedosto&t=119&url=rauheat_esite_hin-nasto_2019_lowres&type=pdf; 2019 [accessed December 2021].
- [51] Fortum. Pörssi-sähköä - niin kuin sinä sen haluat. <https://www.fortum.fi/kotiasiakkailla/sahkoa-kotiin/sahkosopimukset/tarkka-porssisahko>; 2019 [accessed December 2021].
- [52] Caruna Espoo Oy. Verkkopalveluhinnasto. https://images.caruna.fi/verkkopalveluhinnasto_caruna_espoo_oy_1.7.2018_2021.pdf; 2018 [accessed December 2021].
- [53] Fortum. Lähisähkö. <https://www.fortum.fi/kotiasiakkailla/sahkoa-kotiin/uusiutuva-energia/oman-tuotannon-myynti-lahisahko>; 2019 [accessed December 2021].
- [54] Motiva. CO2 emission factors. <https://www.motiva.fi/ratkaisut/energiankaytto-suomessa/co2-paastokertoimet>; 2019 [accessed December 2021].
- [55] Finlex. Emission trading law. <https://www.finlex.fi/fi/laki/ajantasa/2011/20110311>; 2011 [accessed December 2021].
- [56] Refinitiv. Will high European carbon prices last? <https://www.refinitiv.com/perspectives/market-insights/will-high-european-carbon-prices-last/>; 2018 [accessed December 2021].
- [57] Bua G, Kapp D, Kuik F, Lis E. EU emissions allowance prices in the context of the ECB's climate change action plan. https://www.ecb.europa.eu/pub/economic-bulletin/focus/2021/html/ecb.ebbox202106_05~ef8ce0bc70.en.html; 2021 [accessed February 2022].
- [58] Introduction to Genetic Algorithms. Parameters of GA. <https://www.obitko.com/tutorials/genetic-algorithms/parameters.php>; 1998 [accessed December 2021].